STIFFNESS PARAMETER IDENTIFICATION OF THE MUSCLES OF MASTICATION

A Thesis

by

MICHAEL SCOTT YOUNG

Submitted to the Office of Graduate and Professional Studies of
Texas A&M University
in partial fulfillment of the requirements for the degree of

MASTER OF SCIENCE

Chair of Committee,	Raktim Bhattacharya
Committee Members,	John E. Hurtado
	Michael Madigan
Head of Department,	Rodney Bowersox

August 2016

Major Subject: Aerospace Engineering

ABSTRACT

Oral cancer survivors across the country live with a condition called trismus, or spasm of the jaw muscles, that restricts their ability to perform basic functions such as eating and talking. In order to relieve these patients of their symptoms, we propose a novel wearable device with the capability to adjust to the complete 6 degree of freedom movement of the jaw to perform therapeutic exercises and run real-time diagnostics. These diagnostic can identify certain stiffness parameters that define a patients capabilities of each portion of the 3 closing muscles pairs. Two approaches were implemented i) physician input trajectory and ii) physician input forcing function. For the input trajectory method, a linear least squares approach and a nonlinear least approach were attempted. An extended kalman filter approach was utilized for the force input method.

The results concluded each method is feasible but both depend on the accuracy of the model and initial estimate. The degree of mouth opening dictated the amount of information regarding certain stiffness parameters and dictated the success of each approach. This lays the groundwork for an experimental approach to validate the relevance of certain stiffness parameters in the clinic.

TABLE OF CONTENTS

Page

LIST OF FIGURES

FIGURE Page

LIST OF TABLES

TABLE Page

1. INTRODUCTION

The mouth forms the gateway to social interaction and the basic human activities of talking, eating, or even kissing a loved one. Unfortunately, this becomes severely limited due to a condition called trismus, or spasm of the jaw muscles, that affects millions of people around the world. The cause of trismus can range from trauma, tetanus, developmental disorders, surgery, and others. 5 million patients per year in the United States suffer from trismus, and those patients with the most severe needs are oropharyngeal cancer survivors, as their symptoms are often the most debilitating. Here, the cancer or its subsequent treatment leads to fibrosis of the muscles of mastication or the surrounding tissue. Approximately 150,000 people in the United States currently live with trismus due to oropharyngeal cancer and another 17,800 new patients are diagnosed annually [8] [16]. Although oropharyngeal cancer incidence most frequently stems from smoking and/or alcohol abuse, there is a new emerging and growing demographic of patients whose cancer is caused by the Human Papilloma Virus[9]. Unlike cancer due to tobacco or alcohol use, these patients have better survival outcomes but must live the rest of their lives with the consequences of limited oral function. The adverse effects include reduced nutrition, hindered post treatment follow-up, and compromised routine diagnostic, surgical and dental procedures.

In addition to reduced oral function, trismus can lead to a number of external costs for patients and care providers, resulting in a cascade of implications beyond quality of life. On an average $3.6 billion is spent annually for HNC treatment although it accounts for only 3% of all cancers [2] [32]. Furthermore, treatment costs for HNC patients are, on average, $23,000 higher as compared to other cancers. This

is partially due the fact that HNC survivors require advanced nursing by a factor of 22% as compared to other cancers. These numbers are reflective of the diminished overall health caused by HNC and the detrimental effects of exhaustive treatment. Unfortunately, little information exists surrounding trismus, and current solutions offer little in terms of slowing progression or even reversing the condition.

Currently there are no products on the market that adequately match each patients unique jaw structure. Specifically, the Therabite forces patients to stretch their jaw utilizing a hand operated lever [6]. This device only moves the jaw in two degrees of freedom, unable to account for 6 degrees of freedom and the individual trajectory of motion unique to each human. Similarly, the Dynasplint provides jaw-stretching rehabilitation but is cumbersome and expensive [3]. The device further requires a technician to train both the physician and the patient in device calibration and use. This requirement complicates and delays patient therapy, adding significant frustration to the dubious process of jaw rehabilitation. In fact, many patients and clinicians said they found it very difficult to use the Dynasplint due to its complex design and its non-ergonomic, heavy and cumbersome shape. In other words, patients are left without a solution to manage their condition and physicians lack the tools or information to adequately treat it.

1.1 Research Problem

As mentioned, little is known regarding the root cause of each trismus case. Physicians can palpate the muscles to locate the trouble muscles but most of the musculature remains hidden behind the bone structures. Similarly, this lack of access makes it nearly impossible to place of electromyography sensors on the most of the muscles. Thus, physicians lack the knowledge to adequately assess and treat the condition.

To fill this gap in product offerings, this project will aim to develop a wearable robotic device with actuation and remote sensing capability to perform therapy and identify muscles with severe symptoms. Specifically, the research problem is to develop system identification algorithms to determine stiffness parameters of the muscles of mastication. For an overview of the entire project scope outside this thesis, see the diagram in the appendix (Figure A.1).

1.2 Purpose

Although the ultimate goal is to develop a device that can relieve the symptoms experienced by trismus patients, this work will focus on the diagnostic algorithms that determine the root cause of their condition. The purpose of this work provide insight into each individual's trismus severity so that the physician can assign appropriate therapy via the device or more extensive treatment. Traditionally, system identification has been implemented in robotic arms and aircraft payload applications so the methods are well known. Thus, an assessment will be made as to whether these techniques can be applied to biomechanical systems and, specifically, this diagnostic problem.

1.3 Objectives of the Research

- Design feasible device for rehabilitation and data acquisition
- Identify stiffness parameters of muscles
- Determine maneuvers for minimal error in diagnostics

2. LITERATURE REVIEW

This section will outline the current solutions for trismus, as well as other robotic rehabilitation devices being developed. Additionally, it will look at current parameter estimation methods used for biomechanical systems to date.

2.1 Current Devices

Physicians primarily prescribe two different devices to treat trismus, Dynasplint and Therabite. These are purely mechanical but provide some relief to the patient. As reference, they are shown in Figure 2.1. From discussions with physicians, it is evident that the Therabite is the clinical standard.

(a) Therabite [6]

(b) Dynasplint [3]

Figure 2.1: Current devices prescribed today

Recently, multiple clinical studies [24] compared the efficacy of tongue depressor stretching versus the Therabite and concluded there was not significant difference in improvement while using the device. Consequently, insurance policies changed and

these devices lost the majority of their insurance coverage due to lack of evidence for efficacy of treatment. Based on conversations with physicians at Memorial Sloan Kettering and MD Anderson, other devices can be found on the market but it is rare to find a patient who actually uses them. One device, Therapacer, is electrically actuated using a single motor but is typically used within the hospital setting [7]. This moves strictly up and down without any curvature to adjust for the natural opening of the mouth.

2.2 Robotic Rehabilitation

Significant work in rehabilitation robotics has been completed for the upper and lower extremities. Researchers out of MIT have built an arm rehabilitation apparatus that is successfully used by stroke patients today [4]. Others have been working towards exoskeltons for rehabilitation of gait [30] and arm function [15] after stroke. However, only one Ph.D. dissertation considers a similar approach for the temporomandibular joint (TMJ) [33]. It outlines a hat-like design that can be manually adjusted by the physician or user to better move with the natural trajectory of the jaw. This type of thinking is moving in right direction but still limited itself to the sagittal plane and did not include a diagnostic component.

2.3 System Identification of Biomechanical Systems

Identifcation of joint dynamics and joint parameters plays an important role in the understanding of the human body but also serves to help in the design of improved prosthetic devices that can replicate human motion [25]. Typically, system identification can be split into 3 distinct sections for joint dynamics:

- **Zero Input**: Force and trajectory are observed
- **Position input**: Sense the required force for a certain position input

- **Force or torque input**: Sense the position after an input forcing function

Robert Kearney outlined the state of the art in 1990 to include the aforementioned 3 methods and the pros and cons of each [18]. However, researchers at the time were utilizing primarily 2nd order models to estimate the dynamics of the system. Since the primary use is to design more biologically relevant prosthetics, these methods are sufficient. More recently, models using a Hammerstein model, linear to nonlinear cascade, have been implemented. Westwick and Kearney began to use a separable least squares identification on the ankle[31]. With this, the stretch relfex dynamics could be taken into account but the joint was quantified as a whole rather than on an individual muscle basis. Based on the popularity of the Hammerstein model, several researchers have analyzed iterative solutions to the parameter estimation problem [19] [12].

Some notable work has been completed with direct applications to the jaw. In Cooker's work, the mechanical stiffness of the muscles as group was determined as a function of the frequency of stretching [10]. Another study was performed by Shiller where the jaw impedance was measured in the sagittal plane by applying precise force onto the mandible. The study concluded that stiffness was anisotropic with stiffness greatest along the protrusion-retraction axis and least in the direction of jaw raising and lowering [27].

To the best of the author's knowledge, no significant effort has been undertaken to determine the stiffness parameters of each individual muscle. Furthermore, it appears that there has not been any work to determine the properties of a jaw with trismus, where knowledge of the root cause can play a critical role. This may be due to the inaccuracies involved in the current muscle and articular mechanical models that are discussed in the following section.

2.4 Biomechanics

Biomechanics of muscles, joints, and articular mechanics has been studied extensively throughout the years. The following is a concise review of the relevant literature to describe the temporomandibular joint and the surrounding tissues.

The TMJ performs the unique function of chewing and grinding food which requires rotation and translation movement of the mandible. To perform chewing maneuvers, the mandibular condyle slides about the fossa, shown in Figure 2.2. This allows for various roll, pitch, yaw, lowering/raising, and protrusion/retraction movements of this unique 6 degree of freedom joint.

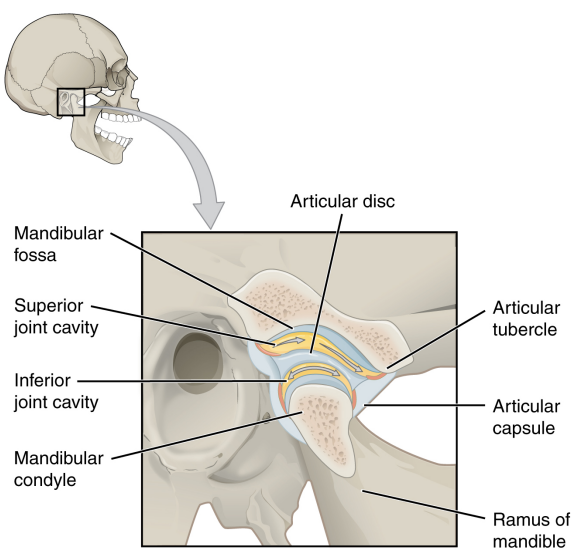

(a) Labeled TMJ [1]

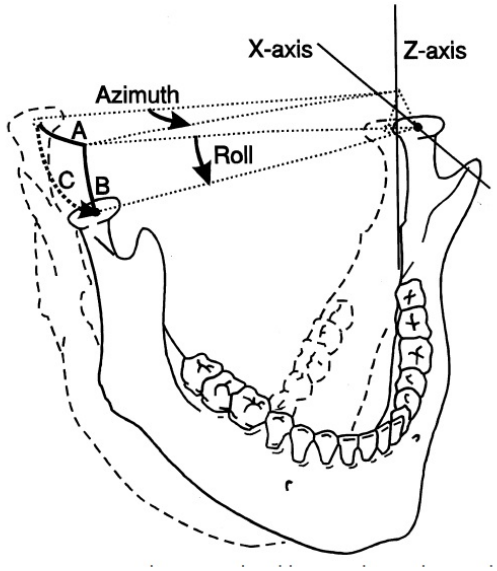

(b) Roll maneuver of TMJ [21]

Figure 2.2: Temporomandibular joint diagrams

In reality, the fossa has curvature in all 3 dimensions, but Koolstrah modeled the fossa as a polynomial plane, depicted in Figure 2.3 and this model closely matches

clinical data [20] [21].

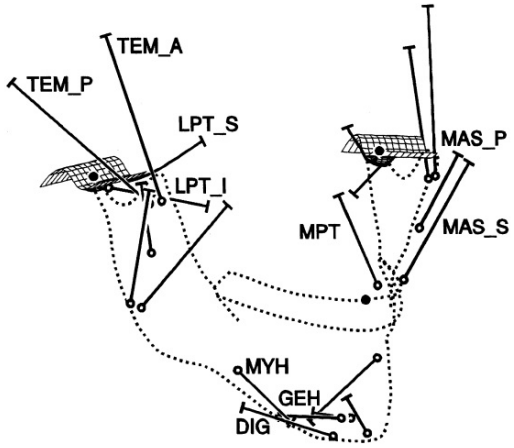

Figure 2.3: Koolstrah's Representation of polynomial fossa with lines of action of various muscle forces

2.4.1 Muscle Mechanics

The muscles of mastication are complex and numerous. It takes 8 muscles on each side of the jaw to perform grinding and circular motions to break down food and some these muscles can be divided into 2 parts. Typically with trismus, only the mouth closing muscles, or those that oppose opening, restrict mouth opening. The primary muscles of concern are the masseter, medial pterygoid, temporalis. Each muscle contains two primary segments and are labeled in Figure 2.4 [13].

Muscles wrap around each other and the bone structures, particularly the temporalis [28]. They also do not act uniformly throughout the length of the muscle, but rather, the strength is a function of cross sectional area [29]. A model utilizing a line of action between the origin point on the maxilla and the insertion point on the skull is seen in many studies and projects, such as the well-known OpenSim [11]

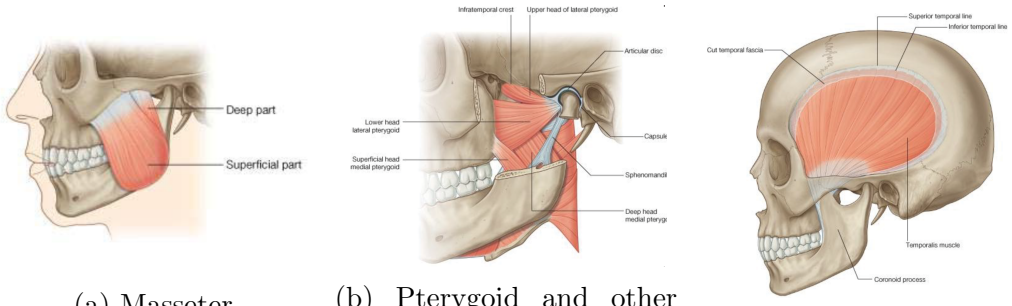

(a) Masseter

(b) Pterygoid and other muscles

(c) Temporalis

Figure 2.4: Labeled muscles of mastication [13]

[20]. OpenSim utilizes this model to realized gait pattern simulations. The issues are important to note[14], but the line of action model serves a starting point for most studies. There is also not a computational efficient model available for most systems and particularly the jaw, although one Parametric Human Project is currently under development [22]. The most commonly used model for line of action forces by muscles is the 1-D Hill-type actuator. This contains elements for force activation FQ, force elongation FL, force velocity FV, and passive force FP as seen in Equation 2.1 [26]. The contractile element consists of a force velocity relation and percent activation component. But since the problem deals with passive resistance to mouth opening, the active forces of the muscles can be neglected to isolate the passive force , F_p

$$F_m = F_{max}(FL \cdot FV \cdot FQ + FP) \tag{2.1}$$

$$FP = a \exp\left(\tilde{b}\frac{SL(t) - SL_o}{SL_o}\right) \tag{2.2}$$

Due to the unethical nature and difficulty in validating the sarcomere length of each person experimentally, it is useful to have a different relation for muscle force.

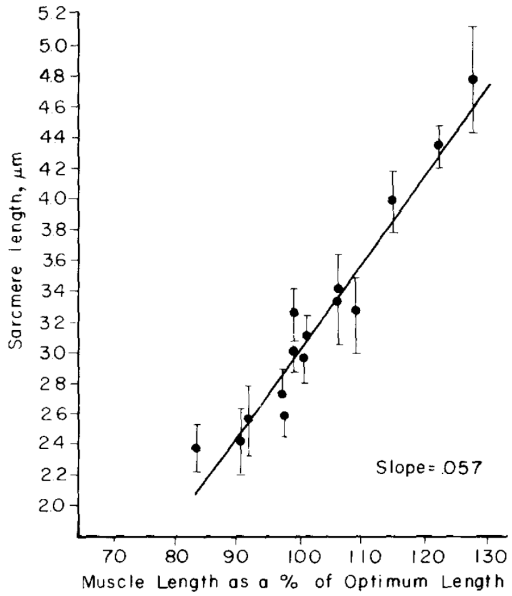

Figure 2.5: Relationship between sarcomere length and change in muscles length [23]

Fortunately, a study outlined the relationship between the sarcomere and change in muscle length as seen in Figure 2.5 [23]. Utilizing the slope of the line, it is straightforward to obtain an equation for sarcomere length.

These relations will be utilize in building the biomechanical model used for this study. All the relevant clinical data regarding muscle positions and parameters can be found in Rujdven's experimental work [29]. A table outline the relevant data is presented in the appendix.

3. DEVICE DESIGN

The purpose of this thesis was to develop the diagnostic algorithms for individual muscle stiffness. Still, it is important to ensure that such a device could be realized in the near future. This section will briefly discuss some of the considerations that went into the concept behind the design as seen in Figure 3.1.

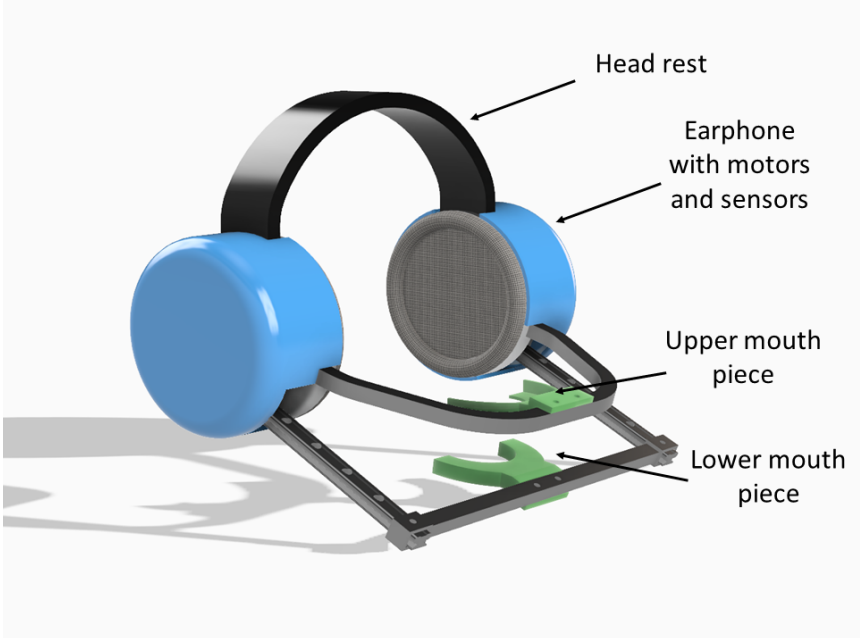

Figure 3.1: Envisioned device design

3.1 Ergonomics

Having informally interviewed 200+ physicians and patients across the country, it is clear that trismus patients require a device that offers multi-tasking capability. Trismus patients undergo therapy, 3 to 7 times a day at upwards of 30 minutes intervals. Since current devices require user-applied hand force, the patient will now

lose almost 2 hours per day just performing therapy in addition to their job and family life.

To overcome this issue, a headphone-like design will provide hands-free autonomous therapy. Headphones are also less conspicuous so the user does not feel embarrassed. The potential acceptability was validated through multiple oral cancer awareness walks and discussions with dental oncologists, maxillofacial surgeons and other physicians in the field.

3.2 6 DOF Capability

Current devices only offer movement in the sagittal plane. In order to perform better diagnostic maneuvers and adjust to the specific structure of each patient, a full 6 DOF device is required. The current design utilizes four motors to actuate the jaw in all directions. To perform the lowering and raising function, a simply hinge joint is required. To compensate for the sliding of the condyle on the fossa, a linear actuation is needed to control the protrusion (forward/backward) movement of the device. Both mechanisms are outlined in Figure 3.2. For yaw or side-to-side movement, a simple sliding slot can be implmented. The jaw does not naturally move side to side with out external force so it does not require actuation. The horizontal actuators will control the yaw of the device that is allowed by this joint..

The motors utilized in this specific configuration are outlined in the following section. It should be noted that other designs may be more optimal. Regardless, the joint configuration described demonstrates the viability of such a device.

3.3 Motor Strength

Data is not present regarding the maximum passive resistance to opening; however, the human biting force ranges from 20-800N, and opening force is 1/20 of closing [24]. For safety, the max resistance is assumed to be 40N. With the above

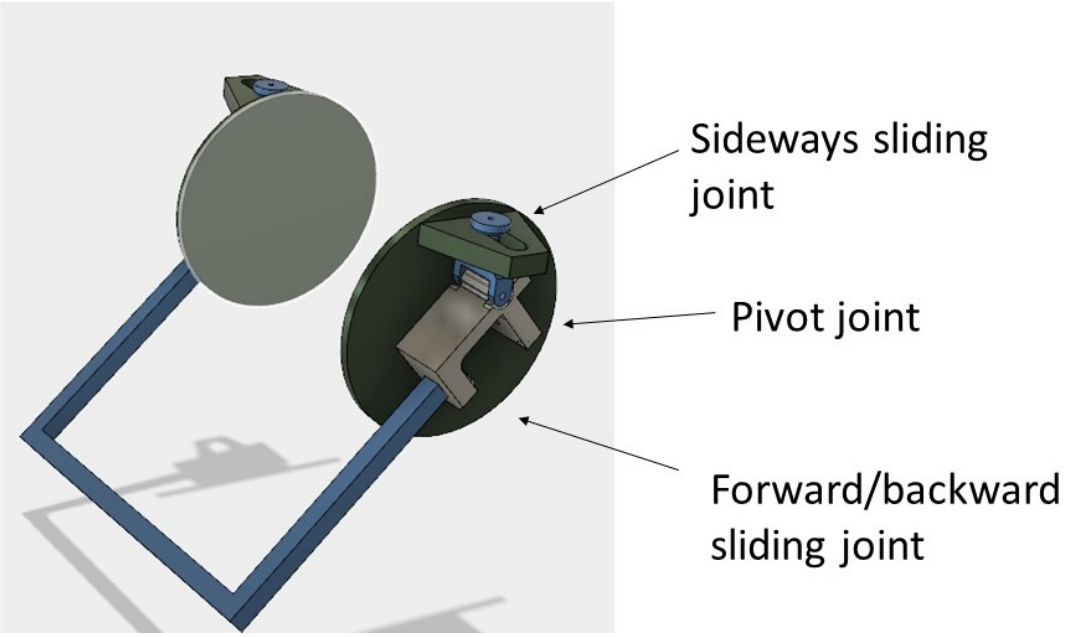

Figure 3.2: Possible 6 degree of freedom joint

configuration, the moment arm length is approximately 12 cm. Thus, the motor needs to have a strength of 160N to overcome the max force. To meet these specs, a NEMA 11 hybrid stepper motor was chosen from KocoMotion with a max thrust force of 230N and a continuous thrust of 150 N [5]. The advantages of the hybrid motor include the small increment in linear actuation and the large holding force to allow for the prescribed optimal passive stretching exercises.

3.4 Data Acquisition

The diagnostic algorithms require the measurement of position and force. Utilizing encoders that pair with the previously described motors are preferable as they have a high accuracy and the implementation is straight forward. To measure the force, it is possible to use the force-velocity relationship that is provided with each motor which would require a lookup table. It is also possible to use a loadcell on the mouthpiece itself or tensile sensors in the headphones.

4. BIOMECHANICAL MODEL

This chapter will walk through the necessary considerations in the construction of the biomechanical model which will be utilized in the derivation of the equations of motion. Following the derivation, a simmechanics model is utilized to verify to dynamics.

4.1 Stiffness Parameters

The literature presents various models for dynamic simulation, but some alterations are necessary for the purpose of this trismus study. As mentioned, the sarcomere length is nearly impossible to validate so Muhl's linear relationship will be utilized, Equation 4.1. This will aid in the formulation of certain stiffness parameters that will be useful to the physician.

$$SL = SL_o + 0.057\frac{\Delta l_m}{l_o} \tag{4.1}$$

$$F_m = F_o \exp\left(b\frac{\Delta l_m}{l_o}\right) \tag{4.2}$$

where $b = \frac{0.057\tilde{b}}{SL_o}$, $F_o = aF_{max}$, $\Delta l_m = l_m(t) - l_o$

$$F_p(t) = F_o \exp(b\frac{l(t) - l_o}{l_o}) \tag{4.3}$$

When F_o is large, the muscle is generally "stiffer" throughout. However, when b is large, the muscle exerts a large force at some percent change in muscle length. Based on discussions with clinicians in the field, it is hypothesized that knowledge of these parameters for each specific muscle will determine if there is a blockage (large b

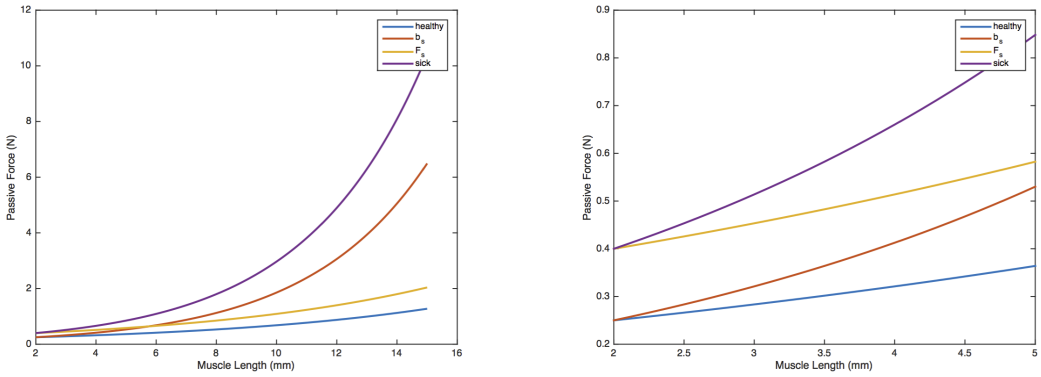

value), i.e. a tumor, that prevents movement or the muscle is becoming increasingly fibrosed (F_o is large). With this, the physician can decide on the next steps in the therapy regime, whether that is surgery, botox injections, or prescription of a robotic therapy device.

4.2 Articular Mechanics

Articular mechanics refers to the joint surface, ligaments, and connective tissue. For the majority of the simulations, this is ignored because these tissues only play a role at the extremities of movement. Since patients experience extreme discomfort at the ends of movement, the device will work to avoid these ranges. However, future studies will be required to identify the properties of articular surfaces since trismus can also arise due to stiffness or shortening of articular tissue.

4.3 Other Tissues

Other tissues surround the muscles and the mandible include the skin, tongue, fat, etc. These provide a damping affect on the dynamics and are modeled generally as simple damping moment $c\boldsymbol{\omega}$. This could also include some of articular mechanics. This component of the equation creates a more realistic model which will a smoother response with an input force. Since there is not any data that assigns a number to

c, an arbitrary value is assigned to replicate motion as seen in real life.

4.4 Kinematics

Before moving into the dynamics, it is useful to understand the kinematics associated with the human jaw model that incorporates Koolstrah's planar fossa. The points of interest are the origin point o, point of contact between the condyle and maxilla $*$, center of gravity of the mandible c.g. , and the location of the applied force a, which are labeled in Figure 4.2. Unless otherwise specified by $[\cdot]_b$, all vector quantities are represented in the inertial frame and measured from point o. The position and velocity of the condyle on the fossa, $\boldsymbol{r}_*$ and $\boldsymbol{v}_*$ respectively, is derived using the Koolstrah's planar model and the curvature is a sinusoidal function. Then, the body angular rate $\boldsymbol{\omega}$ is used to determine the velocity at the center of gravity and applied force.

$$\boldsymbol{r}_* = \begin{bmatrix} x(t) \\ y(t) \\ d(\cos(fx(t)) - 1) \end{bmatrix} \tag{4.4}$$

$$\boldsymbol{r}_a = \boldsymbol{r}_* + (\boldsymbol{r}_a - \boldsymbol{r}_*) \tag{4.5}$$

$$\boldsymbol{r}_a - \boldsymbol{r}_* = \boldsymbol{C} \cdot [\boldsymbol{r}_{*a}]_b \tag{4.6}$$

Taking the derivative and utilizing transport theorem:

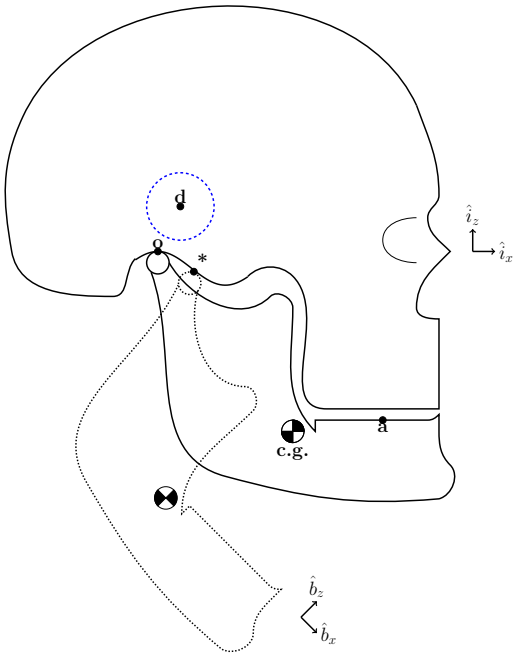

Figure 4.2: Side view (Sagittal plane) of mandible movement with labeled points of interest

$$\boldsymbol{v}_* = \begin{bmatrix} \dot{x} \\ \dot{y} \\ \dot{x} - df\sin(fx) \end{bmatrix} \tag{4.7}$$

$$\boldsymbol{v}_c = \boldsymbol{v}_* + \boldsymbol{\omega} \times (\boldsymbol{r}_c - \boldsymbol{r}_*) \tag{4.8}$$

Since $\boldsymbol{r}_{\text{c.g.}} - \boldsymbol{r}_*$ is a constant value, the notation will $r_{*/c}$ will use used to denote the vector from the moving point $*$ to the center of gravity. Using the product rule

yields the result

$$\boldsymbol{v}_{\text{c.g.}} = \boldsymbol{v}_* + \boldsymbol{\omega} \times \boldsymbol{r}_{*/c} \tag{4.9}$$

$$\boldsymbol{a}_{\text{c.g.}} = \boldsymbol{a}_* + \dot{\boldsymbol{\omega}} \times \boldsymbol{r}_{*/c} + \boldsymbol{\omega} \times (\boldsymbol{\omega} \times \boldsymbol{r}_{*/c}) \tag{4.10}$$

The euler kinematics are described with a 2-3-1 rotation.

Starting with the Euler Angle Kinematics from a 2-3-1 rotation though θ, ψ, and α.

$$[\boldsymbol{v}]_b = \boldsymbol{C}_{2,3,1}(\theta, \psi, \alpha)[\boldsymbol{v}]_i \tag{4.11}$$

$$\boldsymbol{\omega} = [\dot{\alpha}, 0, 0]^T + \boldsymbol{C}_1(\alpha)[0, 0, \dot{\psi}]^T + \boldsymbol{C}_1(\alpha)\boldsymbol{C}_3(\psi)[0, \dot{\theta}, 0]^T \tag{4.12}$$

$$\boldsymbol{\omega} = \underbrace{\begin{bmatrix} 1 & \sin(\psi) & 0 \\ 0 & \cos(\alpha)\cos(\psi) & \sin(\alpha) \\ 0 & -\sin(\alpha)\cos(\psi) & \cos(\alpha) \end{bmatrix}}_{\boldsymbol{B}} \dot{\boldsymbol{u}} \tag{4.13}$$

$$\dot{\boldsymbol{u}} = \boldsymbol{A}\boldsymbol{\omega} \tag{4.14}$$

where $\boldsymbol{A} = \boldsymbol{B}^{-1}$

With this rotation scheme, the singularity occurs at $\psi = \pi/2$. Physically, this is when the jaw is 90° sideways so it is safe to assume that the system will never reach or approach this value.

4.5 Dynamics

Combining the passive resistance, line of action muscle with the derived kinematics, the conservation of angular momentum Eq. 4.17 can be used to derive the dynamics of the system [17].

$$\boldsymbol{h}_c = \boldsymbol{I}_c \boldsymbol{\omega} \tag{4.15}$$

$$\boldsymbol{\varsigma}_* = \boldsymbol{h}_c + (\boldsymbol{r}_c - \boldsymbol{r}_*) \times m\boldsymbol{v}_c \tag{4.16}$$

$$\dot{\boldsymbol{\varsigma}}_* = \boldsymbol{l}_* + m\boldsymbol{v}_c \times \boldsymbol{v}_* \tag{4.17}$$

$$\boldsymbol{l}_* = \sum_{i=1}^{M} \boldsymbol{r}_{m_i} \times \boldsymbol{F}_{m_i}(t) + \boldsymbol{r}_a \times \boldsymbol{F}_a(t) \tag{4.18}$$

$$\tag{4.19}$$

Where F_a is the known applied force by the device onto the jaw and F_{m_i} is the i^{th} muscle force described in Eq. 4.3.

$$\dot{\boldsymbol{\varsigma}}_* = m\boldsymbol{v}_{\text{c.g.}} \times \boldsymbol{v}_* + \boldsymbol{r}_a \times \boldsymbol{F}_a(t) + \sum_{i=1}^{M} \boldsymbol{r}_{m_i} \times \boldsymbol{F}_{m_i}(t) \tag{4.20}$$

$$\dot{\boldsymbol{\varsigma}}_* = \boldsymbol{I}_c \dot{\boldsymbol{\omega}} + \boldsymbol{\omega} \times (\boldsymbol{I}_c \boldsymbol{\omega}) + m\left[\boldsymbol{r}_{*/c} \times \boldsymbol{a}_{\text{c.g.}} + \boldsymbol{\omega} \times (\boldsymbol{r}_{*/c} \times \boldsymbol{v}_{\text{c.g.}})\right] \tag{4.21}$$

Plugging in $\boldsymbol{a}_{\text{c.g.}}$

$$\begin{aligned} \dot{\boldsymbol{\varsigma}}_* = \boldsymbol{I}_c \dot{\boldsymbol{\omega}} + \boldsymbol{\omega} \times (\boldsymbol{I}_c \boldsymbol{\omega}) + m[\boldsymbol{r}_{*/c} \times (\boldsymbol{a}_* + \dot{\boldsymbol{\omega}} \times \boldsymbol{r}_{*/c} + \boldsymbol{\omega} \times (\boldsymbol{\omega} \times \boldsymbol{r}_{*/c})) \\ + \boldsymbol{\omega} \times (\boldsymbol{r}_{*/c} \times \boldsymbol{v}_{\text{c.g.}})] \end{aligned} \tag{4.22}$$

$$\begin{aligned} \boldsymbol{I}_c \dot{\boldsymbol{\omega}} + m\boldsymbol{r}_{*/c} \times (\dot{\boldsymbol{\omega}} \times \boldsymbol{r}_{*/c}) = m\boldsymbol{v}_{\text{c.g.}} \times \boldsymbol{v}_* + \boldsymbol{r}_a \times \boldsymbol{F}_a(t) + \sum_{i=1}^{M} \boldsymbol{r}_{m_i} \times \boldsymbol{F}_{m_i}(t) \\ - \boldsymbol{\omega} \times (\boldsymbol{I}_c \boldsymbol{\omega}) - m[\boldsymbol{r}_{*/c} \times (\boldsymbol{a}_* + \boldsymbol{\omega} \times (\boldsymbol{\omega} \times \boldsymbol{r}_{*/c})) + \boldsymbol{\omega} \times (\boldsymbol{r}_{*/c} \times \boldsymbol{v}_{\text{c.g.}})] \end{aligned} \tag{4.23}$$

A is equal to the following:

$$\boldsymbol{A} = \boldsymbol{I}_c - m[\boldsymbol{r}^X_{*/c}][\boldsymbol{r}^X_{*/c}] \tag{4.24}$$

Now solving for $\dot{\boldsymbol{\omega}}$ a simple solution for the dynamics can be derived:

$$\begin{aligned}\dot{\boldsymbol{\omega}} = \boldsymbol{A}^{-1}\{m\boldsymbol{v}_{\text{c.g.}} \times \boldsymbol{v}_* + \boldsymbol{r}_a \times \boldsymbol{F}_a(t) + \sum_{i=1}^{M} \boldsymbol{r}_{m_i} \times \boldsymbol{F}_{m_i}(t) \\ -\boldsymbol{\omega} \times (\boldsymbol{I}_c\boldsymbol{\omega}) - m[\boldsymbol{r}_{*/c} \times (\boldsymbol{a}_* + \boldsymbol{\omega} \times (\boldsymbol{\omega} \times \boldsymbol{r}_{*/c})) + \boldsymbol{\omega} \times (\boldsymbol{r}_{*/c} \times \boldsymbol{v}_{\text{c.g.}})\}\end{aligned} \tag{4.25}$$

Now, it is possible to derive the dynamics for the point along the condyle utlizing Newton's 2nd Law. For notation, $\boldsymbol{N}$ is the normal force on the condyle from the fossa, which is unknown. However, knowledge of the shape and the fact that it acts normal to the plane will allow for isolation of the desired terms.

$$\boldsymbol{F} = m\boldsymbol{a}_c \tag{4.26}$$

$$\boldsymbol{N} + \sum \boldsymbol{F}_{m_i} + \boldsymbol{F}_a = m(\boldsymbol{a}_* + \dot{\boldsymbol{\omega}} \times \boldsymbol{r}_{*/c} + \boldsymbol{\omega} \times (\boldsymbol{\omega} \times \boldsymbol{r}_{*/c})) \tag{4.27}$$

$$\begin{aligned}\frac{1}{|\boldsymbol{p}|}\boldsymbol{C}\underbrace{\begin{bmatrix} -d(\cos(fx) - 1) \\ 0 \\ x \end{bmatrix}}_{\boldsymbol{p}} = m\boldsymbol{a}_* - m^2\boldsymbol{A}^{-1}(\boldsymbol{r}_{*/c} \times \boldsymbol{a}_*) \times \boldsymbol{r}_{*/c} + \\ m\boldsymbol{A}^{-1}\{m\boldsymbol{v}_{\text{c.g.}} \times \boldsymbol{v}_* + \boldsymbol{l}_* - \boldsymbol{\omega} \times (\boldsymbol{I}_c\boldsymbol{\omega}) - m[\boldsymbol{r}_{*/c} \times (\boldsymbol{\omega} \times (\boldsymbol{\omega} \times \boldsymbol{r}_{*/c})) + \\ \boldsymbol{\omega} \times (\boldsymbol{r}_{*/c} \times \boldsymbol{v}_{\text{c.g.}})]\} \times \boldsymbol{r}_{*/c} + m\boldsymbol{\omega} \times (\boldsymbol{\omega} \times \boldsymbol{r}_{*/c}) - \sum \boldsymbol{F}\end{aligned} \tag{4.28}$$

Using some shorthand notation to isolate $\boldsymbol{a}_*$ and N from the remaining terms

grouped in $\boldsymbol{S}$:

$$N\boldsymbol{C}\hat{\boldsymbol{p}} = \underbrace{m(I_{3x3} + mA^{-1}[\boldsymbol{r}^X_{*/c}][\boldsymbol{r}^X_{*/c}])}_{\boldsymbol{Q}}\boldsymbol{a}_* + \boldsymbol{s} \tag{4.29}$$

$$N\underbrace{\boldsymbol{Q}^{-1}\boldsymbol{C}\hat{\boldsymbol{p}}}_{\boldsymbol{v}} = \boldsymbol{a}_* + \boldsymbol{Q}^{-1}\boldsymbol{s} \tag{4.30}$$

$$N\begin{bmatrix} v_x \\ v_y \\ v_z \end{bmatrix} = \begin{bmatrix} \ddot{x} \\ \ddot{y} \\ -\ddot{x}fd\sin(fx) - \dot{x}f^2d\cos(fx) \end{bmatrix} + \underbrace{\boldsymbol{Q}^{-1}\boldsymbol{s}}_{\boldsymbol{s}} \tag{4.31}$$

Subtracting the x-component times v_z from the z component times v_x will eliminate N and allow isolation of $\ddot{x}$.

$$0 = \ddot{x}v_z + (\ddot{x}fd\sin(fx) + \dot{x}^2f^2d\cos(fx))v_x + s_xv_z - s_zv_x \tag{4.32}$$

$$\ddot{x} = \frac{1}{v_z + v_xfd\sin(fx)}(s_zv_x - s_xv_z - v_x\dot{x}^2f^2d\cos(fx)) \tag{4.33}$$

The same method can be used to isolate $\ddot{y}$

$$0 = v_x\ddot{y} - v_y\ddot{x} + v_xs_y - v_ys_x \tag{4.34}$$

$$\ddot{y} = \frac{1}{v_x}(v_y\ddot{x} - v_xs_y + v_ys_x) \tag{4.35}$$

4.6 Simmechanics Model

To validate the dynamics for simulation, a 6 degree of freedom model was constructed in MATLAB's Simmechanics software package. Below is brief outline of

how this was constructed that was based on some existing work cited previously. An overview of the entire model is located in the appendix. This will go over some of the improvements and information lacking in the literature.

4.7 Joint

The most significant contribution is the development of the sliding mechanism in Simmechanics. Previous models in Simmechanics only dealt in the sagital plane; however, the use of a prismatic joint normal to the fossa plane allows for lateral sliding, as seen in Figure 4.3.

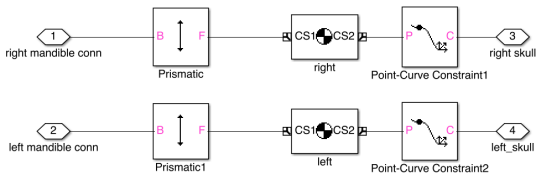

Figure 4.3: Simmechanics condyle model

4.8 Muscles

The muscles are attached with 3 degree of freedom joints at the origin and insertion points on the maxilla and mandible, respectively, as seen in Figure 4.4. The force is calculated using body sensors and the equations to describe passive force derived previously.

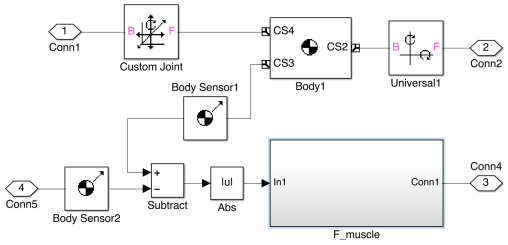

Figure 4.4: Simmechanics muscle model

5. SYSTEM IDENTIFICATION

Previously, 3 primary methods for system identification of biomechanical systems were outlined. For trismus patients, it is likely that the physician will want to prescribe a therapy regime based on a slow passive mouth opening over a long period of time, or input the trajectory and sense the input force. However, it is also possible that the physician will want to control the input force in order to maintain a certain level of comfort and not overwork the muscles. Thus, both approaches are examined. A lineariziation method and monte carlo/ non-linear least squares approaches are attempted for the trajectory input and an extended kalman filter approach is outlined for the force input. The pros and cons of each are outlined in the discussion section, but this section will walk through their respective derivations.

Unknown	Measured	Assumed Known
$\boldsymbol{r}_*, \boldsymbol{v}_*, \boldsymbol{a}_*$	$\boldsymbol{r}_a, \boldsymbol{v}_a, \boldsymbol{a}_a$	m, $\boldsymbol{I}_c, [\boldsymbol{r}_{\text{c.g.}}]_b$
ψ, θ, ϕ, $\boldsymbol{\omega}$, $\dot{\boldsymbol{\omega}}$	$\boldsymbol{F}_a$	f, d
$\boldsymbol{p}$		$[\boldsymbol{r}_a - \boldsymbol{r}_*]_b$, $\boldsymbol{r}_{m_i}$, $\boldsymbol{r}_{m_i}$

Table 5.1: Summary of known and unknown information

For the scope of this project, it is assumed that the kinematic properties of the TMJ are known, such as condyle shape, mandible size, and approximate center of gravity for the mandible. This assumption is acceptable due to the ease of access to MRI images and image processing techniques. Surgical planning software companies already extract this information from the MRI images; however, future work will aim to reduce these assumptions. For notation, the parameters of interest are the stiffness parameters $\boldsymbol{p} = [F_{m_1}, b_1, ..., F_{m_M}, b_M]$. In both approaches, the position,

velocity, and value of the applied force is known whether it is sensed or an input. The unknowns are the position of the condyle on the mandible, the euler angles, the body angle rates, and the unknown stiffness parameters (summarized in Table 5.1).

5.1 Inverse Kinematics of Mandible Position

The system identification algorithms that determine the desired parameters, $\boldsymbol{p}$, require knowledge of the position of the condyle on the fossa $\boldsymbol{r}_*$. Since it is not possible to measure this in real time, inverse kinematic techniques will be pursued to determine these values based on the input trajectory.

$$[\boldsymbol{r}_a]_i = [\boldsymbol{r}_{*_1}]_i + \boldsymbol{C}(\psi, \theta, \phi)[(\boldsymbol{r}_a - \boldsymbol{r}_{*_1})]_b \tag{5.1}$$

$$[\boldsymbol{v}_a]_i = [\boldsymbol{v}_{*_1}]_i + \boldsymbol{C}(\psi, \theta, \phi)[\boldsymbol{\omega} \times (\boldsymbol{r}_a - \boldsymbol{r}_{*_1})]_b \tag{5.2}$$

$$[\boldsymbol{a}_a]_i = [\boldsymbol{a}_{*_1}]_i + \boldsymbol{C}(\psi, \theta, \phi)[\dot{\boldsymbol{\omega}} \times (\boldsymbol{r}_a - \boldsymbol{r}_{*_1}) + \boldsymbol{\omega} \times (\boldsymbol{\omega} \times (\boldsymbol{r}_a - \boldsymbol{r}_{*_1}))]_b \tag{5.3}$$

By limiting the bounds, it is possible to find a unique solution that correlates with input trajectory.

5.2 Linearizing the Force Function

In an attempt to find a computationally efficient and simply solution, the passive muscle force was linearized to create a linear least squares problem. The formulation

is outlined below.

$$\dot{\boldsymbol{\varsigma}}_* - \boldsymbol{r}_a \times \boldsymbol{F}_a(t) - m\boldsymbol{v}_c \times \boldsymbol{v}_* = \sum_{i=1}^{M} \boldsymbol{r}_{m_i} \times \boldsymbol{F}_{m_i}(t) \tag{5.4}$$

$$\boldsymbol{g}(\boldsymbol{p}) = \sum_{i=1}^{M} \boldsymbol{r}_{m_i} \times \boldsymbol{F}_{m_i}(t) \tag{5.5}$$

$$= \sum_{i=1}^{M} \underbrace{\boldsymbol{r}_{m_i} \times \hat{\boldsymbol{l}}_i(t)}_{\boldsymbol{a_i}} F_{o_i}(1 + b_i \frac{\Delta|l_i(t)|}{l_o}) \tag{5.6}$$

$$= \sum_{i=1}^{M} \boldsymbol{a}_i \begin{bmatrix} 1 & \frac{\Delta|l_i(t)|}{l_o} \end{bmatrix} \begin{bmatrix} F_{o_i} \\ F_{o_i} b_i \end{bmatrix} \tag{5.7}$$

$$= \sum_{i=1}^{M} \boldsymbol{G}_i(t) \begin{bmatrix} F_{o_i} \\ F_{o_i} b_i \end{bmatrix} \tag{5.8}$$

$$= \begin{bmatrix} \boldsymbol{G}_1(t) & \dots & \boldsymbol{G}_M(t) \end{bmatrix} \begin{bmatrix} F_{o_1} \\ F_{o_1} b_1 \\ \vdots \\ F_{o_M} \\ F_{o_M} b_M \end{bmatrix} \tag{5.9}$$

Since the system is underdefined, multiple time steps, N are required.

$$\begin{bmatrix} \boldsymbol{d}(t_1) \\ \vdots \\ \boldsymbol{d}(t_N) \end{bmatrix} = \begin{bmatrix} \boldsymbol{G}_1(t_1) & \dots & \boldsymbol{G}_M(t_1) \\ \vdots & \ddots & \vdots \\ \boldsymbol{G}_1(t_N) & \dots & \boldsymbol{G}_M(t_N) \end{bmatrix} \begin{bmatrix} F_{o_1} \\ F_{o_1} b_1 \\ \vdots \\ F_{o_M} \\ F_{o_M} b_m \end{bmatrix} \tag{5.10}$$

Now the equation is linear in nature. A pseudo inverse of G will give a linear

least squares answer.

5.3 Generalized Algorithms

Using conservation of angular momentum, Equation 4.17, it is straightforward to isolate the unknown parameters from known data to begin system identification. With this, a nonlinear least squares approximation can be made by minimizing the equations, see the formulation below.

$$\dot{\boldsymbol{\varsigma}}_* - \boldsymbol{r}_a \times \boldsymbol{F}_a(t) - m\boldsymbol{v}_c \times \boldsymbol{v}_* = \sum_{i=1}^{M} \boldsymbol{r}_{m_i} \times \boldsymbol{F}_{m_i}(t) \tag{5.11}$$

$$\boldsymbol{d}(t) = \boldsymbol{g}(\boldsymbol{p}) \tag{5.12}$$

$$\boldsymbol{d}(t) - \boldsymbol{g}(\boldsymbol{p}) = 0 \tag{5.13}$$

Various optimization techniques will be used to minimize the system of equations. Below is a partial problem formulation, where the residual $\boldsymbol{\epsilon}$ is minimized.

$$\boldsymbol{\epsilon}_j = \boldsymbol{g}_j - \boldsymbol{d}_j \tag{5.14}$$

$$f = \sum_{j=1}^{N} ||\boldsymbol{\epsilon}_j||^2 \tag{5.15}$$

Take partials with respect to each unknown variable. Example below:

$$\frac{\partial \boldsymbol{f}}{\partial F_{o_1}} = 2\sum_{j=1}^{N} \begin{bmatrix} \epsilon_j(1)\frac{\partial \epsilon_j(1)}{\partial F_{o_1}} & \epsilon_j(2)\frac{\partial \epsilon_j(2)}{\partial F_{o_1}} & \epsilon_j(3)\frac{\partial \epsilon_j(3)}{\partial F_{o_1}} \end{bmatrix}$$

$$min \begin{bmatrix} \frac{\partial \boldsymbol{f}}{\partial F_{o_1}} \\ \frac{\partial \boldsymbol{f}}{\partial b_1} \\ \vdots \\ \frac{\partial \boldsymbol{f}}{\partial F_{o_M}} \\ \frac{\partial \boldsymbol{f}}{\partial b_M} \end{bmatrix}$$

5.4 Extended Kalman Filter

To address a force input by the physician, an extended kalman filter approach is formulated. This method tracks the Euler angles, body rates, position of the condyle, and stiffness parameters with time.

$$\dot{\boldsymbol{x}}(t) = f(\boldsymbol{x}(t), \boldsymbol{u}(t)) + \boldsymbol{w}(t) \tag{5.16}$$

$$\boldsymbol{z}_k = g(\boldsymbol{x}_k) + \boldsymbol{v}_k \tag{5.17}$$

$$\boldsymbol{x} = \begin{bmatrix} \boldsymbol{u} \\ \boldsymbol{\omega} \\ F_{o_1} \\ b_1 \\ \vdots \\ F_{o_m} \\ b_{o_m} \end{bmatrix}, \quad \boldsymbol{y} = \begin{bmatrix} \boldsymbol{r}_a \\ \boldsymbol{v}_a \end{bmatrix} \tag{5.18}$$

where $\boldsymbol{u} = [\alpha, \theta, \psi]^T$ is the vector of Euler angles.

From the dynamics discussed previously,

$$\begin{aligned} \boldsymbol{f} = \boldsymbol{A}^{-1}\{m\boldsymbol{v}_{\text{c.g.}} \times \boldsymbol{v}_* + \boldsymbol{r}_a \times \boldsymbol{F}_a(t) + \sum_{i=1}^{M} \boldsymbol{r}_{m_i} \times \boldsymbol{F}_{m_i}(t) \\ -\boldsymbol{\omega} \times (\boldsymbol{I}_c\boldsymbol{\omega}) - m[\boldsymbol{r}_{*/c} \times (\boldsymbol{a}_s + \boldsymbol{\omega} \times (\boldsymbol{\omega} \times \boldsymbol{r}_{s/c})) + \boldsymbol{\omega} \times (\boldsymbol{r}_{*/c} \times \boldsymbol{v}_{\text{c.g.}})]\} \end{aligned} \tag{5.19}$$

Going through each individually using the identity, $J(\boldsymbol{a} \times \boldsymbol{b}) = [\boldsymbol{a}^X]J(\boldsymbol{b}) - [\boldsymbol{b}^X]J(\boldsymbol{a})]$

$$\begin{aligned} \boldsymbol{F} = \boldsymbol{A}^{-1}\{m\left([\boldsymbol{v}_{\text{c.g.}}^X]\boldsymbol{J}(\boldsymbol{v}_*) - [\boldsymbol{v}_*^X]\boldsymbol{J}(\boldsymbol{v}_{\text{c.g.}})\right) + \boldsymbol{J}(\boldsymbol{l}_*) - [\boldsymbol{\omega}^X]\boldsymbol{J}(\boldsymbol{I}_{\text{c.g.}}\boldsymbol{\omega}) + [(\boldsymbol{I}_{\text{c.g.}}\boldsymbol{\omega})^X]\boldsymbol{J}(\boldsymbol{\omega}) \\ -m[\boldsymbol{r}_{*/c}^X](\boldsymbol{J}(\boldsymbol{a}_s) + [\boldsymbol{\omega}^X](-[\boldsymbol{r}_{a/c}^X]\boldsymbol{J}(\boldsymbol{\omega})) - [(\boldsymbol{\omega} \times \boldsymbol{r}_{a/c})^X]J(\boldsymbol{\omega})) \\ -m([\boldsymbol{\omega}^X][\boldsymbol{r}_{*/c}^X]\boldsymbol{J}(\boldsymbol{v}_{\text{c.g.}}) - [(\boldsymbol{r}_{*/c} \times \boldsymbol{v}_{\text{c.g.}})^X]\boldsymbol{J}(\boldsymbol{\omega}))\} \end{aligned} \tag{5.20}$$

where

$$J(\boldsymbol{I}_{\text{c.g.}}\boldsymbol{\omega}) = \begin{bmatrix} \boldsymbol{0}_{3\times3} & \boldsymbol{I}_c & \boldsymbol{0}_{3\times2M} \end{bmatrix} \tag{5.21}$$

$$J(\boldsymbol{\omega}) = \begin{bmatrix} \boldsymbol{0}_{3\times3} & \boldsymbol{1}_{3\times3} & \boldsymbol{0}_{3\times2M} \end{bmatrix} \tag{5.22}$$

$$J(\boldsymbol{v}_{\text{c.g.}}) = \boldsymbol{J}(\boldsymbol{C}[\boldsymbol{v}_s]_I) - [\boldsymbol{r}_{s/c}^X]\boldsymbol{J}(\boldsymbol{\omega}) \tag{5.23}$$

$$J(\boldsymbol{v}_*) = \boldsymbol{J}(\boldsymbol{C}[\boldsymbol{v}_s]_I) \tag{5.24}$$

$$J(\boldsymbol{l}_*) = J\left(\boldsymbol{r}_a \times \boldsymbol{F}_a(t) + \sum_{i=1}^{M} \boldsymbol{r}_{m_i} \times \boldsymbol{F}_{m_i}(t)\right) = \begin{bmatrix} J(\boldsymbol{l}_*)_{\boldsymbol{u}} & \boldsymbol{0}_{3\times3} & J(\boldsymbol{l}_*)_{\boldsymbol{p}} \end{bmatrix} \tag{5.25}$$

The length of the muscle is defined as:

$$\boldsymbol{l}_{m_i} = \boldsymbol{r}_{m_o} - \boldsymbol{r}_{m_i} \tag{5.26}$$

$$\boldsymbol{r}_{m_i} = \boldsymbol{r}_s + \boldsymbol{r}_{*/i} \tag{5.27}$$

Putting into the body frame to be consistent

$$\boldsymbol{l}_{m_i} = \boldsymbol{C} \cdot [\boldsymbol{r}_{m_o} - \boldsymbol{r}_*]_I - [\boldsymbol{r}_{*/i}]_b \tag{5.28}$$

$$\begin{aligned} J(\boldsymbol{l}_*)_{\boldsymbol{p}} = \Bigg[\; & \boldsymbol{r}_{m_1} \times \hat{\boldsymbol{l}}_{m_1} \exp\left(b_1 \tfrac{|\boldsymbol{l}_{m_1}| - l_{o_1}}{l_{o_1}}\right) \left[1, F_{o_M} \tfrac{|\boldsymbol{l}_{m_1}| - l_{m_o}}{l_{m_o}}\right] \quad ... \\ ... \quad & \boldsymbol{r}_{m_M} \times \hat{\boldsymbol{l}}_{m_M} \exp\left(b_M \tfrac{|\boldsymbol{l}_{m_M}| - l_{o_M}}{l_{o_M}}\right) \left[1, F_{o_M} \tfrac{|\boldsymbol{l}_{m_M}| - l_{o_M}}{l_{o_M}}\right] \; \Bigg] \end{aligned} \tag{5.29}$$

calculate the jacobian of moment w.r.t $\boldsymbol{u}$

$$\boldsymbol{J}(\boldsymbol{l}_{*_i})_{\boldsymbol{u}} = \left[\boldsymbol{r}_{m_i}^X\right] \boldsymbol{J}_{\boldsymbol{u}} \left(F_{o_i} \exp\left(b_i \frac{|\boldsymbol{l}_m| - l_{o_i}}{l_{o_i}}\right) \hat{\boldsymbol{l}}_{m_i}\right) \tag{5.30}$$

$$= \left[\boldsymbol{r}_{m_i}^X\right] \left\{ F_{o_i} \exp\left(b_i \frac{|\boldsymbol{l}_m| - l_{o_i}}{l_{o_i}}\right) \boldsymbol{J}_{\boldsymbol{u}}(\hat{\boldsymbol{l}}_{m_i}) + \hat{\boldsymbol{l}}_{m_i} \boldsymbol{J}_{\boldsymbol{u}} \left(F_{o_i} \exp\left(b_i \frac{|\boldsymbol{l}_m| - l_{o_i}}{l_{o_i}}\right)\right)\right\} \tag{5.31}$$

$$\hat{\boldsymbol{l}}_m = \frac{\boldsymbol{l}_m}{|\boldsymbol{l}_m|} \tag{5.32}$$

$$|\boldsymbol{l}_m| = \sqrt{l_m(1)^2 + l_m(2)^2 + l_m(3)^2} \tag{5.33}$$

Jacobian for $\hat{\boldsymbol{l}}_m$:

$$\boldsymbol{J}(\hat{\boldsymbol{l}}_m) = \boldsymbol{l}_m \boldsymbol{J}\left(\frac{1}{|\boldsymbol{l}_m|}\right) + \frac{1}{|\boldsymbol{l}_m|}\boldsymbol{J}(\boldsymbol{l}_m) \tag{5.34}$$

$$\boldsymbol{J}(\boldsymbol{l}_m) = \boldsymbol{J}(C \cdot [\boldsymbol{r}_{m_o} - \boldsymbol{r}_*]_I) \tag{5.35}$$

The sensing model

$$[\boldsymbol{r}_a]_I = [\boldsymbol{r}_*]_I + \boldsymbol{C}^T \cdot [\boldsymbol{r}_{*/a}]_b \tag{5.36}$$

$$[\boldsymbol{v}_a]_I = [\boldsymbol{v}_*]_I + \boldsymbol{C}^T \cdot [\boldsymbol{\omega} \times \boldsymbol{r}_{*/a}]_b \tag{5.37}$$

$$\boldsymbol{H} = \begin{bmatrix} \boldsymbol{J_u}(\boldsymbol{C}^T \cdot [\boldsymbol{r}_{*/a}]_b) & \mathbf{0}_{3\times 3} & \mathbf{0}_{3\times 2M} \\ \boldsymbol{J_u}(\boldsymbol{C}^T \cdot [\boldsymbol{\omega} \times \boldsymbol{r}_{*/a}]_b) & -\boldsymbol{C}^T[\boldsymbol{r}^X_{*/a}] & \mathbf{0}_{3\times 2M} \end{bmatrix} \tag{5.38}$$

Using the described jacobians, the EKF implementation is straight forward. One concept worth introducing is observability. By checking the rank of obersvability matrix at certain points for a non-linear system, a reality check can be

6. RESULTS

6.1 Inverse Kinematics

The inverse kinematics provided the position of the condyle on the fossa, which is neccesary information for the estimation of the desired stiffness parameters. As an example, a trajectory including a lowering of the jaw followed by a sideways motion is implemented as seen in Figure 6.1.

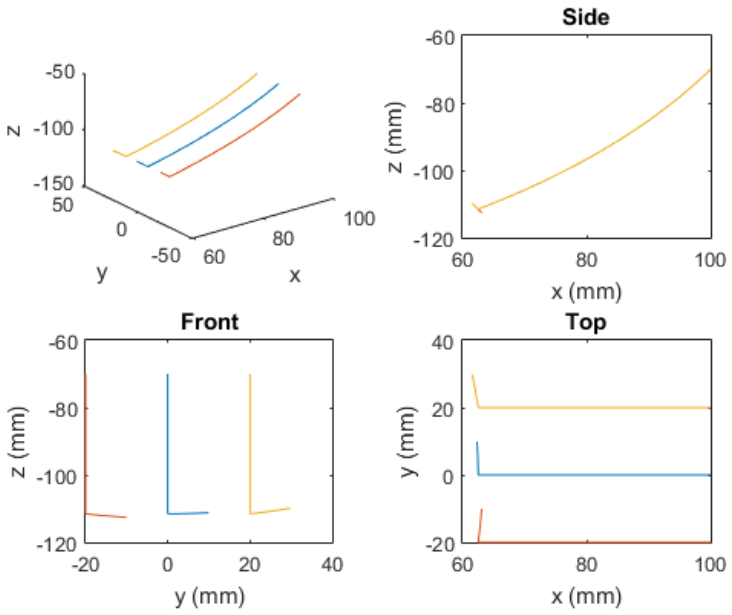

Figure 6.1: Lowering to sideways maneuver, 3 points on mandible

The movement of the condyle on the fossa replicates actual movement of the jaw, as seen in Figure 6.2. However if an aggressive maneuver is prescribed the physician, the algorithm has the potential to fail as it relies on certain bounds of movement. Thus, it would require tuning to adjust for more aggresive therapy. For the case of

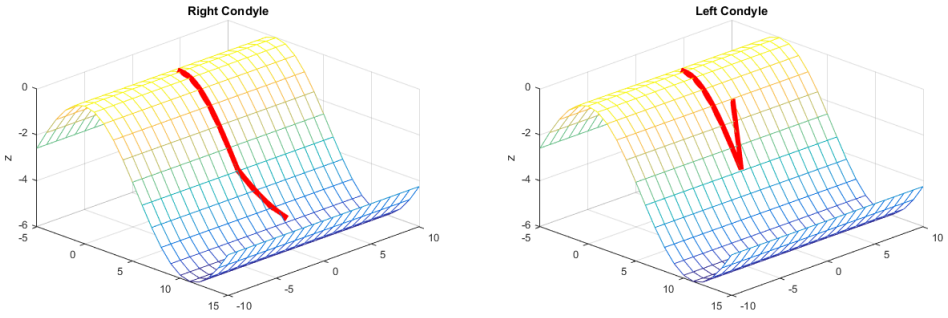

Figure 6.2: Lowering to sideways maneuver, point of contact on fossa with mandible

trismus' slow passive stretches, it will remain sufficient.

6.2 Muscle Linearization Method

Since therapy is conducted upwards of 10 times per day, it is safe to say the at least 10 parameter estimations may take place per day. After 10 days, there will be a total 100 estimates of each parameter. The following results compare the estimates over 100-1000 estimates to determine the mean and standard deviation to serve as an indication of confidence in the approximation. This method of data collection is both for the linearization and generalized versions.

Utilizing a the taylor series linearization of the force muscle, the stiffness parameters were estimated utilizing a linear least squares approach. The results of a 3 degree of freedom model with only 3 muscles is shown in Figure 6.3.

In the estimation for stopping stiffness b, the standard deviation is small while the mean has a large bias. The error of the mean to the true value is much larger than 3σ. Thus, there is little confidence in this method. When more muscles are added, the discrepancy increases so this method was quickly discarded.

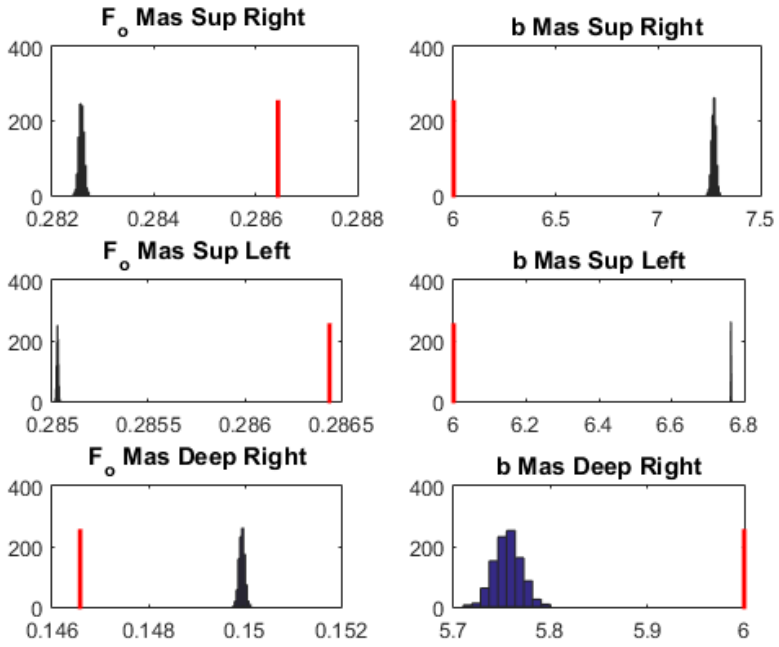

Figure 6.3: Muscle linearization method 3 muscle results Histograms of 1000 simulations with noise

6.3 Generalized Algorithms

Here, the progressive analysis of the algorithm is demonstrated by moving from lower fidelity models to ones with more degrees of freedom and more muscle pairs.

6.3.1 3 Degrees of Freedom

Even with large measurement noise, the mean of the values is close to that of the actual stiffness parameters, as seen in Figure 6.4.

6.4 6 Degrees of Freedom

Figures 6.5 and 6.6 show the raw data collection. For the physician though, this is not useful and a better representation is required. Thus, by collecting all the estimated values for each therapy session, we can average the results and determine

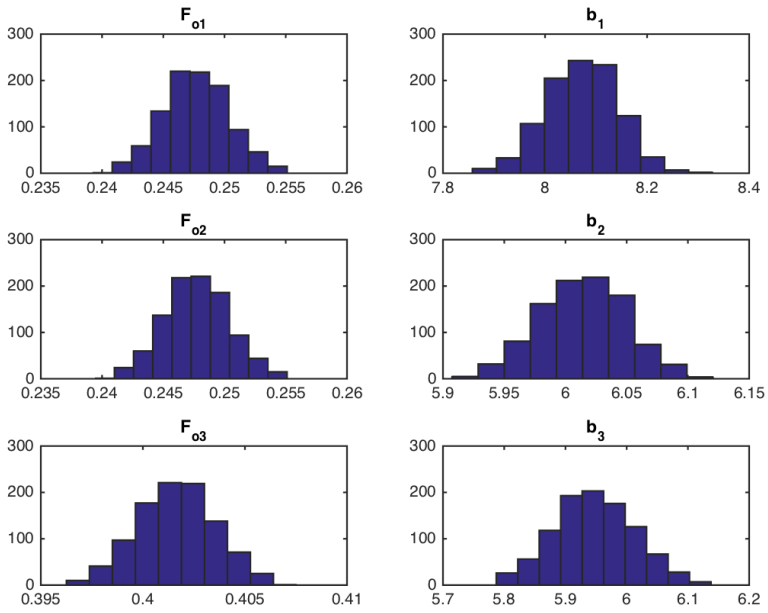

Figure 6.4: Histograms of 1000 simulations with noise. True Values: $F_{o_1} = 0.25$, $b_1 = 8$, $F_{o_2} = 6$, $b_2 = 0.25$, $F_{o_4} = 0.4$, $b_3 = 6$

the standard deviation. This will tell the physician the estimated stiffness values within a certain confidence bound. Examples are shown Figures 6.7 and 6.8.

Here, an enlarged version of the document. As can be seen, the mean is relatively close to the actual value and the standard deviation captures the true value. Since there is not a false indication of healthy when a muscle is sick and vice verse, we have some confidence in this approach.

6.5 Extended Kalman Filter

Several muscle count versions were attempted to understand the limitations of the extended Kalman filter.

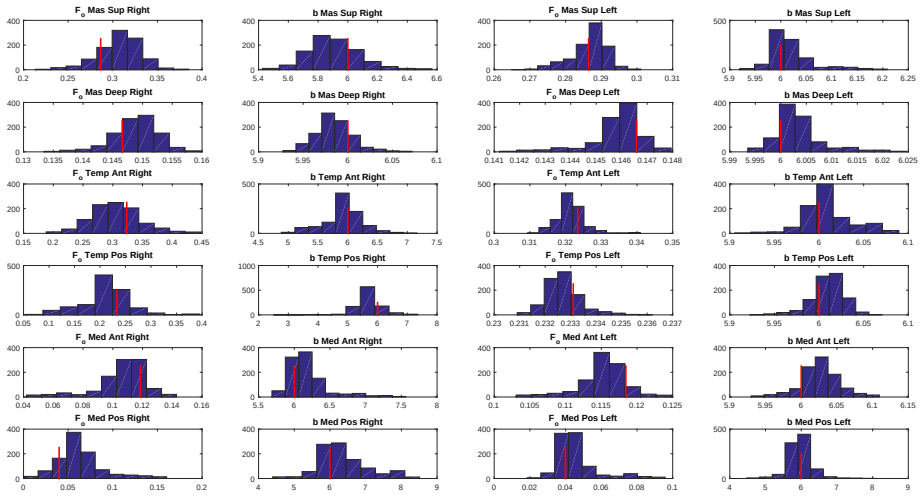

Figure 6.5: 6 degree of freedom, 12 muscle stiffness paramater histogram for non-linear least squares estimation. (1000 estimates plotted)

6.5.1 2 Sided Tracking

By grouping the muscles for each side to characterize stiffness more generally, the extended Kalman filter approach provides converging and accurate results as can be seen in Figures 6.9 and 6.10.

6.5.2 Full Fidelity

By analyzing Figure 6.11, it is possible to track the 12 muscle parameters. Comparing the full muscle model to the 2 sided model, one can see that it does not converge as quickly.

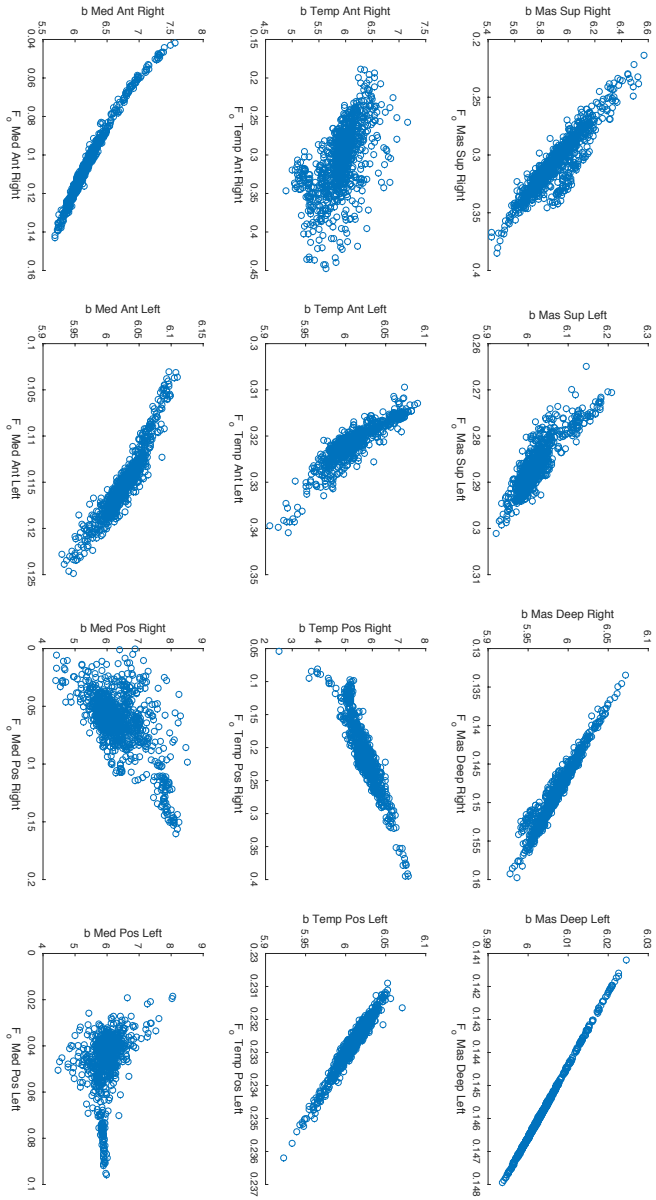

Figure 6.6: Stiffness parameter comparison for the non-linear least squares estimation method (1000 estimates plotted)

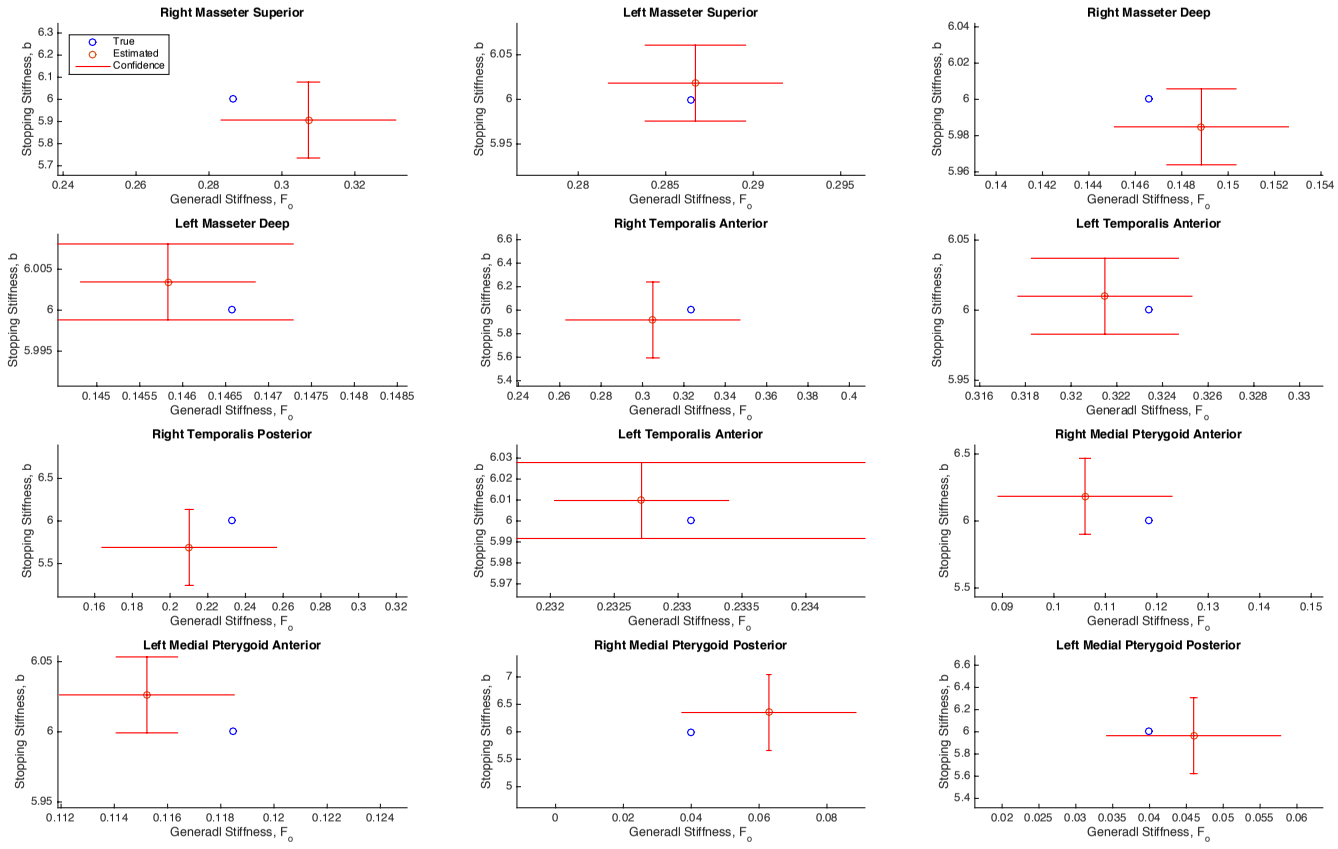

Figure 6.7: Physician view depicting predicted values with a standard deviation bound for each estimate

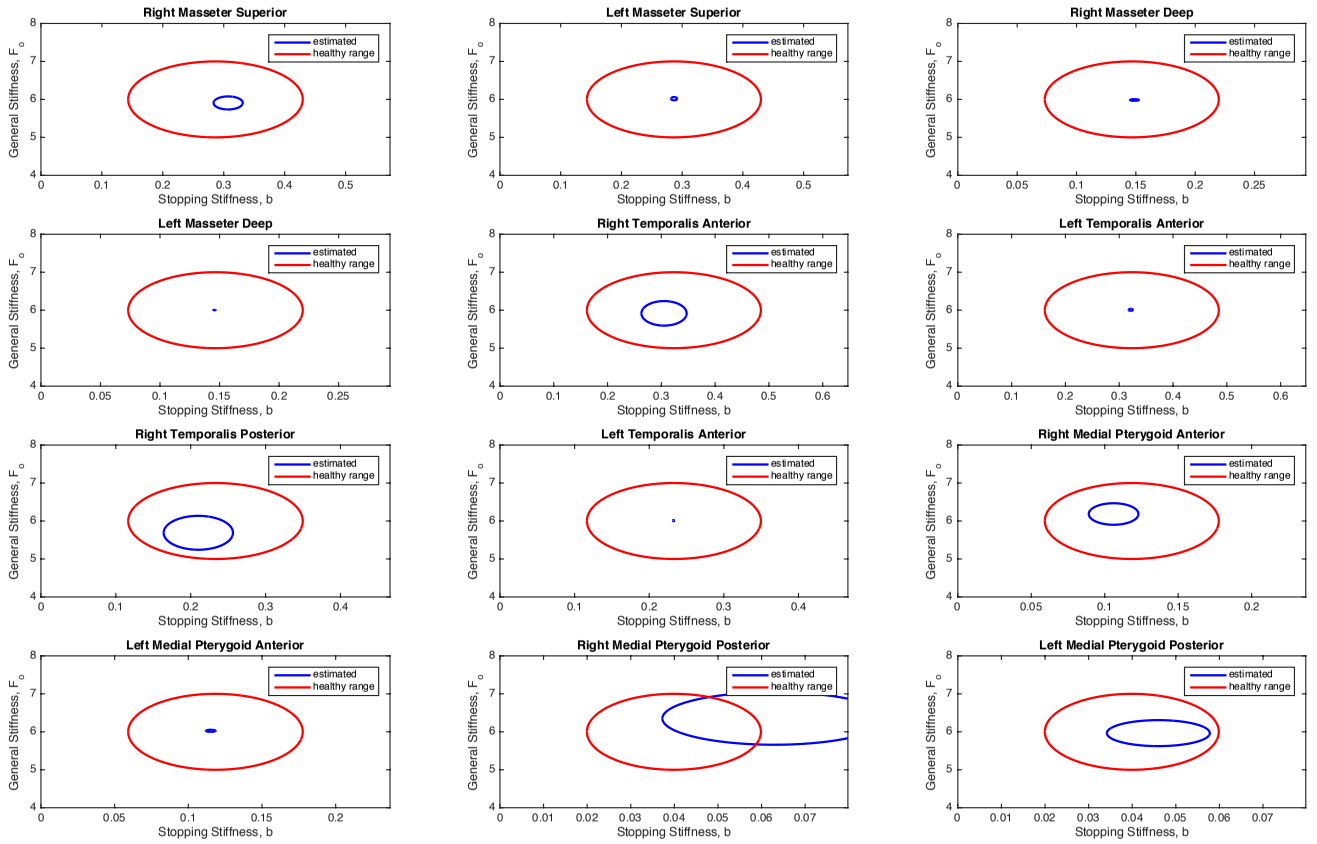

Figure 6.8: Physician view depicting predicted values with a confidence radius bound for each estimate

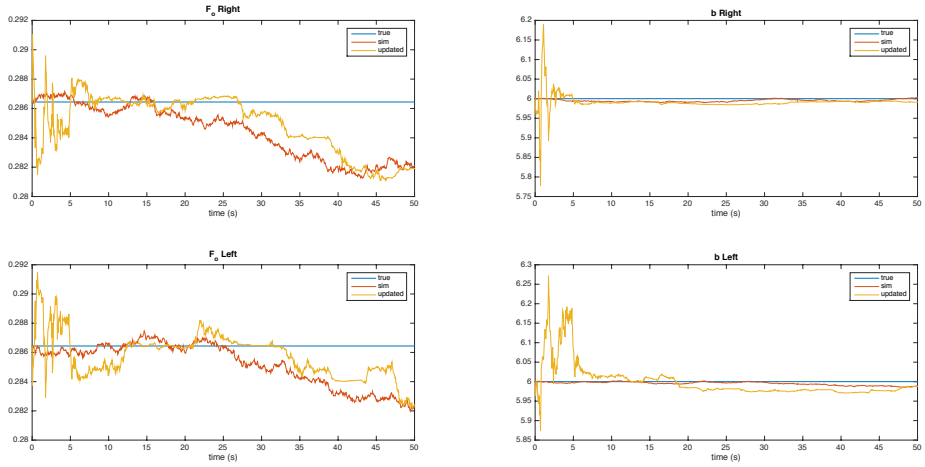

Figure 6.9: Tracking of stiffness parameters for side grouping simulation

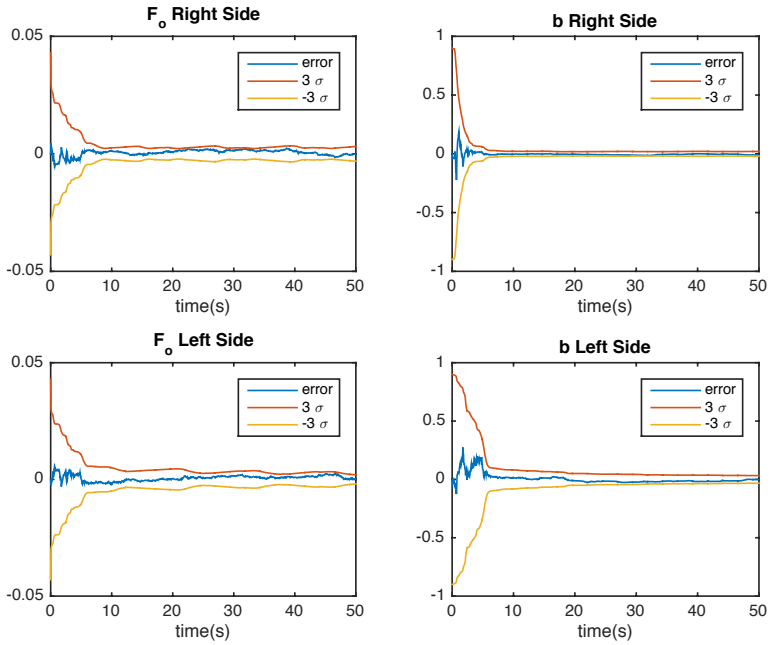

Figure 6.10: Error of simulation tracking 2 muscle groups general stiffness parameters compared to 3σ

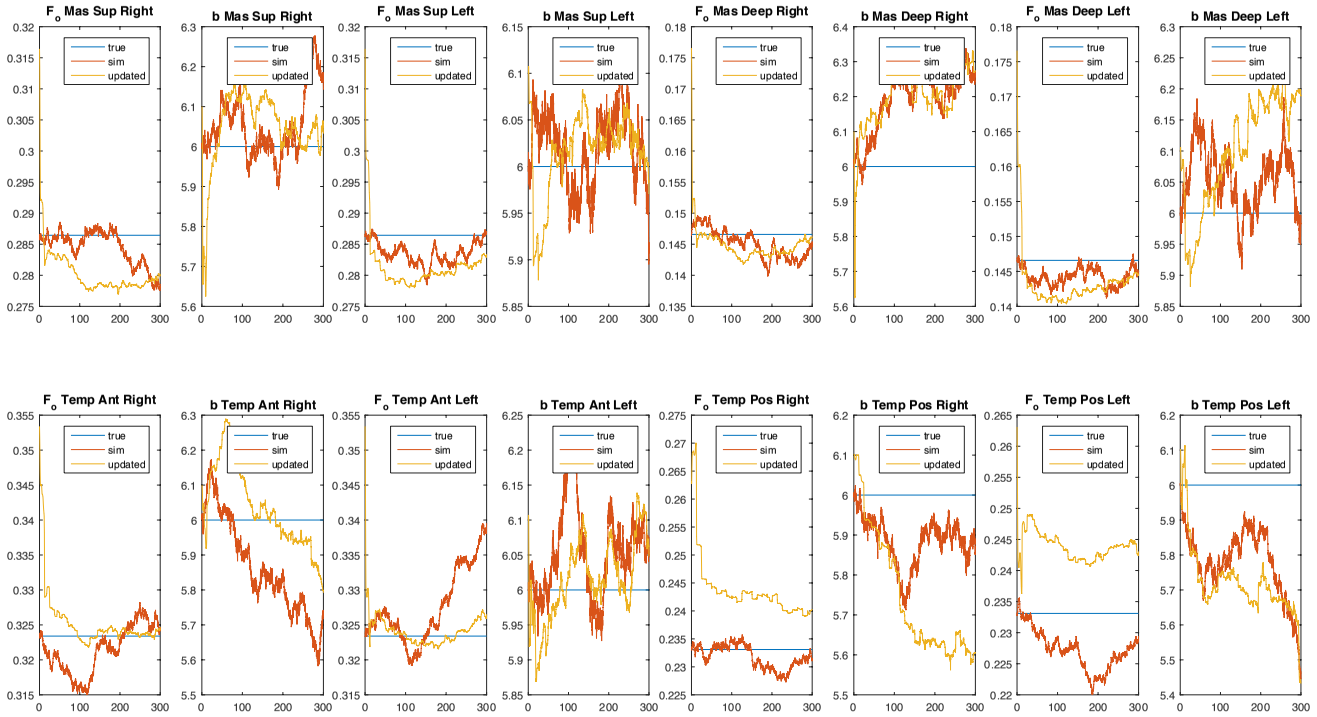

Figure 6.11: Tracking of stiffness parameters for multiple muscles

7. DISCUSSION

7.1 Maneuver

Since the muscles are model as exponential functions, it is obvious that little information is provided regarding the parameter b when the change in muscle length is small. Oppositely, it is easy to predict F_o at small deflection. When maneuvers were performed that did not exceed 10 degrees of mouth opening, both the extended kalman filter and the Monte Carlo methods produced poor estimations of b without having a reliable guess.

When more muscles were added to the simulations, more complex maneuvers were required to determine the muscle noise. In other words, moving the jaw left and right allowed to algorithms to converge or find a unique solution more quickly.

7.2 Algorithm Comparison

The first muscle linearization method was used to see if it was possible to generate a closed form solution to the problem. However, the error became too great as muscles were added to the model. Thus, neither muscle linearization method was quickly disregarded and more robust approach was required.

The non-linear least squares optimization method relied on the initial guess and a large amount of computational power. The larger the amount of function evaluations permitted, the more accurate the results if the initial guess was within an acceptable range. Thus, This method will require much more physician training to provide some a priori information regarding which muscles are stiffer than others.

The extended kalman filter provided a more computationally efficient solution and also tracks the movement of the mandible. It takes into account the model error of the muscles of mastication whereas the Monte Carlo simulations rely on the accuracy

of the model, which has its deficiencies as previously discussed. One issue with the Kalman filter approach is the injection of noise onto the constant parameters. Since the parameters are not noticeably changing with each therapy session, they should remain perfectly constant. However, the Kalman filter does not converge without noise injection. Thus, a small noise onto the static parameters is required for the simulation. In application, this should not affect much.

7.3 Future Work

The development of diagnostic algorithms is one small part of a much larger project where a significant amount of work remains. This section will address the primary areas required before clinical trails can commence to assess the efficacy of treatment and diagnosis.

7.3.1 Model Fidelity

Trismus often occurs due to muscle stiffness; however, it can also stem scarring of the tissues inside the mouth or stiffness of the articular surfaces. Thus, it will be necessary to model these more accurately so that relevant diagnostic algorithms can be implemented. In this work, on the passive resistance was modeled. Although this is sufficient in the modeling of trismus, it may happen that the patient has a reflex to stretching that will misguide the diagnostic algorithms. The incorporation of these reflexes will be critical for the successful clinical adoption of such a device.

The proposed stiffness parameters will need to be clinical validated as well. Questions such as: *"Does a higher b value truly mean that muscle has a higher chance of blockage?"* will need to be answer. If higher F_o values relate to the need of more physical therapy versus botox injections, then this will require clinical validation. Thus, a team of clinicians and engineers will need to work together over the next few years to assess these issues.

7.3.2 Experiment Validation

The current algorithms work at a high sampling rate via simulation. Thus, it will be necessary to first tune the algorithms to operate at more realistic, lower sampling rates so that experimental work can occur. This experimental work will involved the reconstruction of the TMJ will force controlled muscle models that operates independently of the device. Then, the device will be tested on this TMJ replica to determine its experimental efficacy.

7.3.3 Eliminate a priori Information

In order to create a more affordable solution, the ideal diagnostic algorithm would not require a priori information regarding muscle position and mandible properties from the MRI images. This will add more static parameters to the estimation problem and the solution is unlikely to converge. Still, further work is required to assess this capability.

7.3.4 Clinical Testing

Before spending months and thousands of dollars on development, it will be important to validate the importance and implications of the stiffness parameters in the clinic. Knowing how they relate to improved outcomes for the patient will be critical in justifying reimbursement. Once the engineering is complete, the proposed solution will require a comparison study to the existing clinical standard to ensure it is as or more effective in treating trismus. Without this validation, patients will not benefit from all the development put into this device.

REFERENCES

[1] Anatomy of selected synovial joints. OpenStax CNX. [Accessed: 2015-06-28], http://cnx.org/contents/R3D4RG6w@4/Anatomy-of-Selected-Synovial-J.

[2] Cancer facts and figures 2015, American Cancer Society. [Accessed: 2015-09-30], http://www.cancer.org/acs/groups/content/@editorial/documents/document/acspc-044552.pdf.

[3] Dynasplint jaw. [Accessed 2015-08-25], http://www.dynasplint.com/divisions/jaw/.

[4] Interactive motion technologies — InMotion ARM interactive therapy system.

[5] Kocomotion, linear acutators. [Accessed: 2015-08-25], http://kocomotionus.com/linear-actuators/.

[6] Therabite jaw rehabilitation system, ATOS Medical. [Accessed: 2015-08-25], http://www.atosmedical.us/product/therabite-jaw-motion-rehabilitation-system/.

[7] Therapacer jaw cpm, Craniorehab. [Accessed: 2015-08-25], http://www.craniorehab.com/orapacer-therapacer-jaw-cpm.html.

[8] Rene-Jean Bensadoun, Dorothea Riesenbeck, Peter B Lockhart, Linda S Elting, Fred KL Spijkervet, Mike T Brennan, et al. A systematic review of trismus induced by cancer therapies in head and neck cancer patients. *Supportive Care in Cancer*, 18(8):1033–1038, 2010.

[9] Anil K Chaturvedi, Eric A Engels, William F Anderson, and Maura L Gillison. Incidence trends for human papillomavirus–related and–unrelated oral squamous cell carcinomas in the united states. *Journal of Clinical Oncology*, 26(4):612–619, 2008.

[10] Harry S Cooker, Charles R Larson, and ES Luschei. Evidence that the human jaw stretch reflex increases the resistance of the mandible to small displacements. *The Journal of Physiology*, 308:61, 1980.

[11] Scott L Delp, Frank C Anderson, Allison S Arnold, Peter Loan, Ayman Habib, Chand T John, Eran Guendelman, and Darryl G Thelen. Opensim: Open-source software to create and analyze dynamic simulations of movement. *Biomedical Engineering, IEEE Transactions on*, 54(11):1940–1950, 2007.

[12] Feng Ding, Xiaoping Peter Liu, and Guangjun Liu. Identification methods for hammerstein nonlinear systems. *Digital Signal Processing*, 21(2):215–238, 2011.

[13] R. Drake, A. W. Vogl, and A. W. Mitchell. Grays anatomy for students. 2009.

[14] Alan G Hannam and Anne S McMillan. Internal organization in the human jaw muscles. *Critical Reviews in Oral Biology & Medicine*, 5(1):55–89, 1994.

[15] Sarah J Housman, Vu Le, Tariq Rahman, Robert J Sanchez, and David J Reinkensmeyer. Arm-training with t-wrex after chronic stroke: preliminary results of a randomized controlled trial. In *Rehabilitation Robotics, 2007. ICORR 2007. IEEE 10th International Conference on*, pages 562–568. IEEE, 2007.

[16] Krapcho M. Garshell J. Miller D. Altekruse S.F. Kosary C.L. Yu M. Ruhl J. Tatalovich Z. Mariotto A. Lewis D.R. Chen H.S. Feuer E.J. Howlade N, Noone A.M. and Cronin K.A. (eds). Seer cancer statistics review (csr) 1975-2012.

[17] John E Hurtado. *Kinematic and Kinetic Principles*. Lulu. com, 2012.

[18] Robert E Kearney and Ian W Hunter. System identification of human joint dynamics. *Critical Reviews in Biomedical Engineering*, 18(1):55–87, 1989.

[19] Robert E Kearney, Richard B Stein, and Luckshman Parameswaran. Identification of intrinsic and reflex contributions to human ankle stiffness dynamics. *Biomedical Engineering, IEEE Transactions on*, 44(6):493–504, 1997.

[20] Jan Harm Koolstra. Dynamics of the human masticatory system. *Critical Reviews in Oral Biology & Medicine*, 13(4):366–376, 2002.

[21] JH Koolstra and TMGJ Van Eijden. Three-dimensional dynamical capabilities of the human masticatory muscles. *Journal of Biomechanics*, 32(2):145–152, 1999.

[22] Digital Human Modeling. Parametric human project. [Accessed: 2015-09-01], parametrichuman.org.

[23] ZF Muhl, AF Grimm, and PL Glick. Physiologic and histologic measurements of the rabbit digastric muscle. *Archives of Oral Biology*, 23(12):1051–1059, 1978.

[24] Nina Pauli. Treating radiation-induced trismus in head and neck cancer; exercise intervention and risk structures. **(Doctoral Thesis), University of Gothenburg, Sweden, 2015.**

[25] Elliott J Rouse, Levi J Hargrove, Eric J Perreault, and Todd A Kuiken. Estimation of human ankle impedance during walking using the perturberator robot. In *Biomedical Robotics and Biomechatronics (BioRob), 2012 4th IEEE RAS & EMBS International Conference on*, pages 373–378. IEEE, 2012.

[26] L. J. Ruijven and W. A. Weijs. A new model for calculating muscle forces from electromyograms. *European Journal of Applied Physiology and Occupational Physiology*, 61(5):479–485.

[27] Douglas M Shiller, Rafael Laboissière, and David J Ostry. Relationship between jaw stiffness and kinematic variability in speech. *Journal of Neurophysiology*, 88(5):2329–2340, 2002.

[28] Jan Harm Koolstrah Theo MGJ van Eijden and Peter Brugman. Three-dimensional structure of the human temporalis muscle. *The Anatomical Record*, 246:565–572, 1996.

[29] TMGJ Van Eijden, JAM Korfage, and P Brugman. Architecture of the human jaw-closing and jaw-opening muscles. *The Anatomical Record*, 248(3):464–474, 1997.

[30] Jan F Veneman, Rik Kruidhof, Edsko EG Hekman, Ralf Ekkelenkamp, Edwin HF Van Asseldonk, and Herman Van Der Kooij. Design and evaluation of the lopes exoskeleton robot for interactive gait rehabilitation. *Neural Systems and Rehabilitation Engineering, IEEE Transactions on*, 15(3):379–386, 2007.

[31] David T Westwick and Robert E Kearney. Separable least squares identification of nonlinear hammerstein models: Application to stretch reflex dynamics. *Annals of Biomedical Engineering*, 29(8):707–718, 2001.

[32] Erika Wissinger, Ingolf Griebsch, Juliane Lungershausen, Talia Foster, and Chris L Pashos. The economic burden of head and neck cancer: a systematic literature review. *Pharmacoeconomics*, 32(9):865–882, 2014.

[33] Wang Xiaoyun. A novel wearable assistive device for jaw motion disability. (Doctoral Dissertation) Massey University, Auckland, New Zealand, 2014.

APPENDIX A

FIRST APPENDIX

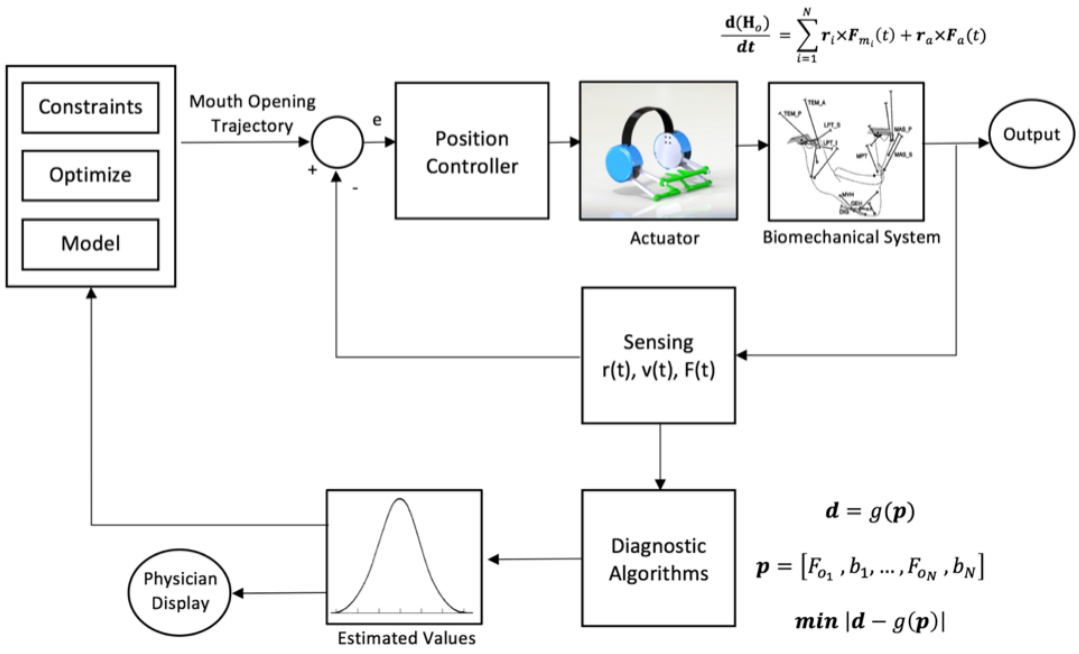

Figure A.1: Top-level description of overall project (This work focuses on diagnostic algorithms box of flow chart)

A.1 Alternative EKF Derivation

$$\boldsymbol{v}_{\text{c.g.}} = \boldsymbol{v}_a + \boldsymbol{\omega} \times \boldsymbol{r}_{a/c} \tag{A.1}$$

$$\boldsymbol{a}_{\text{c.g.}} = \boldsymbol{a}_a + \dot{\boldsymbol{\omega}} \times \boldsymbol{r}_{a/c} + \boldsymbol{\omega} \times (\boldsymbol{v}_a + \boldsymbol{\omega} \times \boldsymbol{r}_{c/a}) \tag{A.2}$$

Plug in $\boldsymbol{a}_{\text{c.g.}}$ with $\boldsymbol{a}_a$ into equation 4.21 in order to separate $\dot{\boldsymbol{\omega}}$:

$$\begin{aligned}\dot{\boldsymbol{\varsigma}}_* = \boldsymbol{I}_c\dot{\boldsymbol{\omega}} + \boldsymbol{\omega} \times (\boldsymbol{I}_c\boldsymbol{\omega}) + m[\boldsymbol{r}_{*/c} \times (\boldsymbol{a}_a + \dot{\boldsymbol{\omega}} \times \boldsymbol{r}_{a/c} + \boldsymbol{\omega} \times (\boldsymbol{v}_a + \boldsymbol{\omega} \times \boldsymbol{r}_{a/c}))\\ +\boldsymbol{\omega} \times (\boldsymbol{r}_{*/c} \times \boldsymbol{v}_{\text{c.g.}})]\end{aligned} \tag{A.3}$$

$$\begin{aligned}\boldsymbol{I}_c\dot{\boldsymbol{\omega}} + m\boldsymbol{r}_{*/c} \times (\dot{\boldsymbol{\omega}} \times \boldsymbol{r}_{a/c}) = m\boldsymbol{v}_{\text{c.g.}} \times \boldsymbol{v}_* + \boldsymbol{r}_a \times \boldsymbol{F}_a(t) + \sum_{i=1}^{M} \boldsymbol{r}_{m_i} \times \boldsymbol{F}_{m_i}(t)\\ -\boldsymbol{\omega} \times (\boldsymbol{I}_c\boldsymbol{\omega}) - m[\boldsymbol{r}_{*/c} \times (\boldsymbol{a}_a + \boldsymbol{\omega} \times (\boldsymbol{v}_a + \boldsymbol{\omega} \times \boldsymbol{r}_{a/c})) + \boldsymbol{\omega} \times (\boldsymbol{r}_{*/c} \times \boldsymbol{v}_{\text{c.g.}})]\end{aligned} \tag{A.4}$$

Looking at just the left hand side:

$$\boldsymbol{I}_c\dot{\boldsymbol{\omega}} + m\boldsymbol{r}_{*/c} \times (\dot{\boldsymbol{\omega}} \times \boldsymbol{r}_{a/c}) = \boldsymbol{A}\dot{\boldsymbol{\omega}} \tag{A.5}$$

$$\boldsymbol{A} = \boldsymbol{I}_c - m[\boldsymbol{r}^X_{*/c}][\boldsymbol{r}^X_{a/c}] \tag{A.6}$$

$$\begin{aligned}\dot{\boldsymbol{\omega}} = \boldsymbol{A}^{-1}\{m\boldsymbol{v}_{\text{c.g.}} \times \boldsymbol{v}_* + \boldsymbol{r}_a \times \boldsymbol{F}_a(t) + \sum_{i=1}^{M} \boldsymbol{r}_{m_i} \times \boldsymbol{F}_{m_i}(t)\\ -\boldsymbol{\omega} \times (\boldsymbol{I}_c\boldsymbol{\omega}) - m[\boldsymbol{r}_{*/c} \times (\boldsymbol{a}_a + \boldsymbol{\omega} \times (\boldsymbol{v}_a + \boldsymbol{\omega} \times \boldsymbol{r}_{a/c})) + \boldsymbol{\omega} \times (\boldsymbol{r}_{*/c} \times \boldsymbol{v}_{\text{c.g.}})\}\end{aligned} \tag{A.7}$$

$$\begin{aligned}\boldsymbol{f} = \boldsymbol{A}^{-1}\{m\boldsymbol{v}_{\text{c.g.}} \times \boldsymbol{v}_* + \boldsymbol{r}_a \times \boldsymbol{F}_a(t) + \sum_{i=1}^{M} \boldsymbol{r}_{m_i} \times \boldsymbol{F}_{m_i}(t)\\ -\boldsymbol{\omega} \times (\boldsymbol{I}_c\boldsymbol{\omega}) - m[\boldsymbol{r}_{*/c} \times (\boldsymbol{a}_a + \boldsymbol{\omega} \times (\boldsymbol{v}_a + \boldsymbol{\omega} \times \boldsymbol{r}_{a/c})) + \boldsymbol{\omega} \times (\boldsymbol{r}_{*/c} \times \boldsymbol{v}_{\text{c.g.}})]\}\end{aligned} \tag{A.8}$$

$$\boldsymbol{F} = \boldsymbol{A}^{-1}\{m\left([\boldsymbol{v}^X_{\text{c.g.}}]\boldsymbol{J}(\boldsymbol{v}_*) - [\boldsymbol{v}^X_*]\boldsymbol{J}(\boldsymbol{v}_{\text{c.g.}})\right) + \boldsymbol{J}(\boldsymbol{l}_*) - [\boldsymbol{\omega}^X]\boldsymbol{J}(\boldsymbol{I}_{\text{c.g.}}\boldsymbol{\omega}) + [(\boldsymbol{I}_{\text{c.g.}}\boldsymbol{\omega})^X]\boldsymbol{J}(\boldsymbol{\omega})$$
$$-m[\boldsymbol{r}^X_{*/c}](\boldsymbol{J}(\boldsymbol{a}_a) + [\boldsymbol{\omega}^X](\boldsymbol{J}(\boldsymbol{v}_a) - [\boldsymbol{r}^X_{a/c}]\boldsymbol{J}(\boldsymbol{\omega})) - [(\boldsymbol{v}_a + \boldsymbol{\omega} \times \boldsymbol{r}_{a/c})^X]J(\boldsymbol{\omega}))$$
$$-m([\boldsymbol{\omega}^X][\boldsymbol{r}^X_{*/c}]\boldsymbol{J}(\boldsymbol{v}_{\text{c.g.}}) - [(\boldsymbol{r}_{*/c} \times \boldsymbol{v}_{\text{c.g.}})^X]\boldsymbol{J}(\boldsymbol{\omega}))\} \tag{A.9}$$

$$J(\boldsymbol{v}_{\text{c.g.}}) = \boldsymbol{J}(\boldsymbol{C}[\boldsymbol{v}_a]_I) - [\boldsymbol{r}^X_{a/c}]\boldsymbol{J}(\boldsymbol{\omega}) \tag{A.10}$$

$$J(\boldsymbol{v}_*) = \boldsymbol{J}(\boldsymbol{C}[\boldsymbol{v}_a]_I) - [\boldsymbol{r}^X_{a/*}]\boldsymbol{J}(\boldsymbol{\omega}) \tag{A.11}$$

$$\boldsymbol{l}_{m_i} = \boldsymbol{r}_{m_o} - \boldsymbol{r}_{m_i} \tag{A.12}$$

$$\boldsymbol{r}_{m_i} = \boldsymbol{r}_a + \boldsymbol{r}_{a/i} \tag{A.13}$$

$$\boldsymbol{l}_{m_i} = \boldsymbol{C} \cdot [\boldsymbol{r}_{m_o} - \boldsymbol{r}_a]_I - [\boldsymbol{r}_{a/i}]_b \tag{A.14}$$

Convoluted method. Delete later

$$\boldsymbol{J}(\boldsymbol{l}_{*_i})_{\boldsymbol{u}} = \left[\boldsymbol{r}_{m_i} F_{o_i} \exp\left(b_i \frac{|\boldsymbol{l}_m| - l_{o_i}}{l_{o_i}}\right)^X\right] \boldsymbol{J}_{\boldsymbol{u}}(\hat{\boldsymbol{l}}_{m_i}) - [\hat{\boldsymbol{l}}_{m_i}^X] \boldsymbol{J}_{\boldsymbol{u}}\left(\boldsymbol{r}_{m_i} F_{o_i} \exp\left(b_i \frac{|\boldsymbol{l}_m| - l_{o_i}}{l_{o_i}}\right)\right) \tag{A.15}$$

$$\boldsymbol{J}_{\boldsymbol{u}}\left(\boldsymbol{r}_{m_i} F_{o_i} \exp\left(b_i \frac{|\boldsymbol{l}_m| - l_{o_i}}{l_{o_i}}\right)\right) = F_{o_i} \boldsymbol{r}_{m_i} \boldsymbol{J}_{\boldsymbol{u}}\left(\exp\left(b_i \frac{|\boldsymbol{l}_m| - l_{o_i}}{l_{o_i}}\right)\right) \tag{A.16}$$

$$\hat{\boldsymbol{l}}_m = \frac{\boldsymbol{l}_m}{|\boldsymbol{l}_m|} \tag{A.17}$$

$$|\boldsymbol{l}_m| = \sqrt{l_m(1)^2 + l_m(2)^2 + l_m(3)^2} \tag{A.18}$$

Using the chain rule and $\boldsymbol{J}(l_{o_i}) = 0$

$$= F_{o_i} \frac{b_i}{l_{o_i}} \exp\left(b_i \frac{|\boldsymbol{l}_{m_i}| - l_{o_i}}{l_{o_i}}\right) \boldsymbol{r}_{m_i} \cdot \boldsymbol{J}_{\boldsymbol{u}}(|\boldsymbol{l}_{m_i}|) \tag{A.19}$$

Knowing that $\boldsymbol{J}(a \cdot b) = b\boldsymbol{J}(a) + a\boldsymbol{J}(b)$ with the following identities:

$$\frac{\partial}{\partial x}\sqrt{f(x)} = \frac{\frac{\partial f}{\partial x}}{2\sqrt{f(x)}}, \quad \frac{\partial}{\partial x}\left(\frac{1}{\sqrt{f(x)}}\right) = -\frac{\frac{\partial f(x)}{\partial x}}{2f(x)^{3/2}}, \quad \frac{\partial}{\partial x} f(x)^2 = 2f(x)\frac{\partial f(x)}{\partial x} \tag{A.20}$$

The jacobians for $\hat{\boldsymbol{l}}_m$ and $|\boldsymbol{l}_m|$ are derived:

$$\frac{\partial}{\partial x}(|\boldsymbol{l}_m|) = \frac{1}{|\boldsymbol{l}_m|}\left(l_m(1)\frac{\partial l_m(1)}{\partial x} + l_m(2)\frac{\partial l_m(2)}{\partial x} + l_m(2)\frac{\partial l_m(2)}{\partial x}\right) \tag{A.21}$$

$$\boldsymbol{J}_{\boldsymbol{u}}(|\boldsymbol{l}_m|) = \begin{bmatrix} \frac{\partial(l_m)}{\partial \alpha} & \frac{\partial(l_m)}{\partial \theta} & \frac{\partial(l_m)}{\partial \phi} \end{bmatrix} \tag{A.22}$$

$$\boldsymbol{J}(\hat{\boldsymbol{l}}_m) = \boldsymbol{l}_m \boldsymbol{J}\left(\frac{1}{|\boldsymbol{l}_m|}\right) + \frac{1}{|\boldsymbol{l}_m|}\boldsymbol{J}(\boldsymbol{l}_m) \tag{A.23}$$

$$\boldsymbol{J}(\boldsymbol{l}_m) = \boldsymbol{J}(C \cdot [\boldsymbol{r}_{m_o} - \boldsymbol{r}_a]_I) \tag{A.24}$$

A.2 1 DOF EKF

Single degree of freedom formulation:

$$\dot{\boldsymbol{x}} = \begin{bmatrix} \omega \\ -\frac{1}{I_o}(r_a F_a + r_m F_o \exp\left(b\frac{l_m(t)-l_o}{l_o}\right)\sin(\beta) \\ 0 \\ 0 \end{bmatrix} + \boldsymbol{w}(t) \tag{A.25}$$

$$\beta = \sin^{-1}\left(\frac{r_o \sin(\theta)}{l_m}\right), \quad l_m = \sqrt{r_o^2 + r_m^2 - 2 r_m r_o \cos(\theta)} \tag{A.26}$$

$$\boldsymbol{y} = \begin{bmatrix} r_a\cos(\theta) \\ -r_a\sin(\theta) \\ -r_a\omega\sin(\theta) \\ -r_a\omega\cos(\theta) \end{bmatrix} + \boldsymbol{v}(t) \tag{A.27}$$

$$\boldsymbol{F} = \left.\frac{\partial \boldsymbol{f}}{\partial \boldsymbol{x}}\right|_{\hat{\boldsymbol{x}}(t),\boldsymbol{u}(t)} \tag{A.28}$$

$$-\frac{1}{I_o}\begin{bmatrix} 0 & -I_o & 0 & 0 \\ f_{21} & 0 & r_m \exp\left(b\frac{l_m-l_o}{l_o}\right)\sin(\beta) & r_m F_o \frac{l_m-l_o}{l_o} exp\left(b\frac{l_m-l_o}{l_o}\right) sin(\beta) \\ 0 & 0 & 0 & 0 \\ 0 & 0 & 0 & 0 \end{bmatrix} \tag{A.29}$$

$$\boldsymbol{G} = \left.\frac{\partial \boldsymbol{g}}{\partial \boldsymbol{x}}\right|_{\hat{\boldsymbol{x}}(t)} \tag{A.30}$$

$$- \begin{bmatrix} -r_a \sin(\theta) & 0 & 0 & 0 \\ -r_a \cos(\theta) & 0 & 0 & 0 \\ -r_a \omega \cos(\theta) & -r_a \sin(\theta) & 0 & 0 \\ 0 & 0 & 0 & 0 \end{bmatrix} \tag{A.31}$$

A.3 Long Equations for EKF Derivation

General form of a repeated Jacobian in the derivation.

$$J(\boldsymbol{Cr})_{\boldsymbol{u}} = \begin{bmatrix} 0 & \dots \\ r_1(c(\alpha)s(\theta) + c(\theta)s(\alpha)s(\psi)) + r_3(c(\alpha)c(\theta) - s(\alpha)s(\theta)s(\psi)) - r_2 c(\psi)s(\alpha) & \dots \\ -r_1(s(\alpha)s(\theta) - c(\alpha)c(\theta)s(\psi)) - r_3(c(\theta)s(\alpha) + c(\alpha)s(\theta)s(\psi)) - r_2 c(\alpha)c(\psi) & \dots \end{bmatrix}$$

$$\begin{bmatrix} \dots & -r_3 c(\theta)c(\psi) - r_1 c(\psi)s(\theta) & r_2 c(\psi) - r_1 c(\theta)s(\psi) + r_3 s(\theta)s(\psi) \\ \dots & r_1(c(\theta)s(\alpha) + c(\alpha)s(\theta)s(\psi)) - r_3(s(\alpha)s(\theta) - c(\alpha)\cos(\theta)\sin(\psi)) & r_3 c(\alpha)c(\psi)s(\theta) - r_1 c(\alpha)c(\theta)c(\psi) - r_2 c(\alpha)s(\psi) \\ \dots & r_1(c(\alpha)c(\theta) - s(\alpha)s(\theta)s(\psi)) - r_3(c(\alpha)s(\theta) + c(\theta)s(\alpha)s(\psi)) & r_2 s(\alpha)s(\psi) + r_1 c(\theta)c(\psi)s(\alpha) - r_3 c(\psi)s(\alpha)s(\theta) \end{bmatrix}$$

A.4 Failed Method: Maneuver Identification

This method utilizes the properties of the passive muscle force function being an exponential. At small displacement, the force is nearly constant at F_o as seen in Fig. A.2. Thus, the following method utilizes a small angle trajectory to determine F_o for each muscle and then move at a larger trajectory with the estimated values of F_o to solve for the other stiffness parameter b for each muscle. Following, the formulation is laid out.

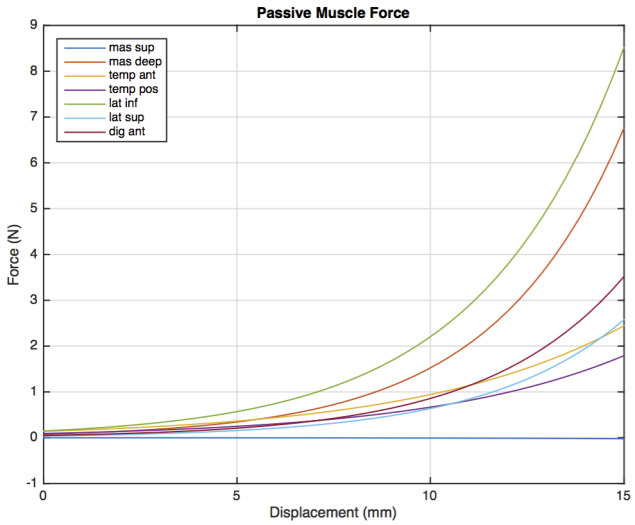

Figure A.2: Passive muscle force of select muscles

$$\dot{\boldsymbol{\varsigma}}_* - \boldsymbol{r}_a \times \boldsymbol{F}_a(t) - m\boldsymbol{v}_c \times \boldsymbol{v}_* = \sum_{i=1}^{M} \boldsymbol{r}_{m_i} \times \boldsymbol{F}_{m_i}(t) \tag{A.32}$$

$$\boldsymbol{g}(\boldsymbol{p}) = \sum_{i=1}^{M} \boldsymbol{r}_{m_i} \times \boldsymbol{F}_{m_i}(t) \tag{A.33}$$

For small mouth opening, it is assumed that the passive muscle force is constant.

$$\boldsymbol{F}_{m_i}(t) = F_{o_i}\hat{\boldsymbol{l}}_i(t) \tag{A.34}$$

$$\boldsymbol{g}(\boldsymbol{p}) = \sum_{i=1}^{M} \underbrace{\boldsymbol{r}_{m_i} \times \hat{\boldsymbol{l}}_i(t)}_{\boldsymbol{a_i}} F_{o_i} \tag{A.35}$$

$$= \left[\begin{array}{c:c:c} \boldsymbol{a}_1(t) & \dots & \boldsymbol{a}_M(t) \end{array}\right] \begin{bmatrix} F_{o_1} \\ \vdots \\ F_{o_M} \end{bmatrix} \tag{A.36}$$

Since the system is underdefined, multiple time steps, N are required.

$$\begin{bmatrix} \boldsymbol{d}(t_1) \\ \vdots \\ \boldsymbol{d}(t_N) \end{bmatrix} = \underbrace{\begin{bmatrix} \boldsymbol{a}_1(t_1) & \dots & \boldsymbol{a}_M(t_1) \\ \vdots & \ddots & \vdots \\ \boldsymbol{a}_1(t_N) & \dots & \boldsymbol{a}_M(t_N) \end{bmatrix}}_{\boldsymbol{H}} \begin{bmatrix} F_{o_1} \\ \vdots \\ F_{o_M} \end{bmatrix} \tag{A.37}$$

By taking the pseudo inverse of $\boldsymbol{H}$, the stiffness parameter F_o is calculated for each muscle. With this approximation, the other stiffness parameter b can be isolated.

$$\boldsymbol{g}(\boldsymbol{p}) = \sum_{i=1}^{M} \boldsymbol{a}_i(t) F_{o_i} \exp(b \frac{\Delta |l_i(t)|}{l_{o_i}}) \tag{A.38}$$

$$= \sum_{i=1}^{M} \boldsymbol{a}_i(t) F_{o_i} \exp(b \frac{\Delta |l_i(t)|}{l_{o_i}}) \tag{A.39}$$

Taking the natural log and putting into matrix form with N data sets as before provides the following:

$$\begin{bmatrix} \boldsymbol{d}(t_1) \\ \vdots \\ \boldsymbol{d}(t_N) \end{bmatrix} = \underbrace{\begin{bmatrix} \ln(\boldsymbol{a}_1(t_1) F_{o_1}) \frac{\Delta |l_1(t_1)|}{l_{o_1}} & \dots & \ln(\boldsymbol{a}_M(t_1) F_{o_M}) \frac{\Delta |l_M(t_1)|}{l_{o_M}} \\ \vdots & \ddots & \vdots \\ \ln(\boldsymbol{a}_1(t_N) F_{o_1}) \frac{\Delta |l_1(t_N)|}{l_{o_1}} & \dots & \ln(\boldsymbol{a}_M(t_N) F_{o_M}) \frac{\Delta |l_M(t_N)|}{l_{o_M}} \end{bmatrix}}_{\boldsymbol{H}} \begin{bmatrix} b_1 \\ \vdots \\ b_M \end{bmatrix} \tag{A.40}$$

Again, a pseduo inverse (or linear least squares) will give an approximation for b for each muscle.

Table A.1: Location of closing muscles

	Origin			Insertion		
	x	y	z	x	y	z
Masseter						
Superficial Part	37.9 ± 0.7	-52.3 ± 3.5	-9.1 ± 1.8	6.2 ± 4.1	-44.9 ± 3.2	-40.7 ± 2.1
Deep Part	30.7 ± 3.7	-48.0 ± 2.0	34.4 ± 3.8	26.4 ± 2.3	-42.6 ± 2.3	-14.8 ± 2.3
Temporalis						
Anterior Part	27.7 ± 2.8	-48.0 ± 2.0	34.4 ± 3.8	26.4 ± 2.3	-42.6 ± 2.3	-14.8 ± 2.3
Posterior Part	-6.2 ± 3.9	-59.3 ± 3.2	32.3 ± 4.4	22.4 ± 1.5	-45.8 ± 2.6	-8.8 ± 2.0
Medial Pterygoid						
Anterior Part	21.2 ± 2.3	-22.3 ± 3.1	-20.5 ± 2.2	2.3 ± 4.5	-39.1 ± 3.3	-48.2 ± 2.5
Posterior Part	20.2 ± 1.4	-14.7 ± 2.4	-9.3 ± 3.7	-2.2 ± 4.3	-40.1 ± 3.1	-37.3 ± 2.9
Lateral Pterygoid						
Inferior Head	19.4 ± 3.5	-24.3 ± 1.9	-14.9 ± 2.4	-0.9 ± 1.4	-46.1 ± 2.0	-3.1 ± 2.8
Superior Head	23.0 ± 3.9	-24.2 ± 2.9	6.4 ± 3.8	0.2 ± 2.1	-44.1 ± 3.1	0.5 ± 2.4